Communications on Applied Mathematics and Computation (2025) 7:1146–1173
https://doi.org/10.1007/s42967-024-00469-9

ORIGINAL PAPER

Energy-Conserving Hermite Methods for Maxwell's Equations

Daniel Appelö [1] · **Thomas Hagstrom** [2] · **Yann-Meing Law** [3]

Received: 22 January 2024 / Revised: 23 June 2024 / Accepted: 12 August 2024 /
Published online: 26 February 2025

Abstract
Energy-conserving Hermite methods for solving Maxwell's equations in dielectric and dispersive media are described and analyzed. In three space dimensions, methods of order $2m$ to $2m+2$ require $(m+1)^3$ degrees-of-freedom per node for each field variable and can be explicitly marched in time with steps independent of m. We prove the stability for time steps limited only by domain-of-dependence requirements along with error estimates in a special semi-norm associated with the interpolation process. Numerical experiments are presented which demonstrate that Hermite methods of very high order enable the efficient simulation of the electromagnetic wave propagation over thousands of wavelengths.

Keywords Maxwell's equations · High-order methods · Hermite methods

Mathematics Subject Classification 65M70

1 Introduction

Hermite methods are general-purpose discretization schemes for solving time-dependent partial differential equations exploiting the unique projection properties of the Hermite-Birkhoff interpolation [2]. Hermite methods are particularly well-suited for hyperbolic equations for two reasons.

- In contrast with typical polynomial-based element methods, Hermite methods for hyperbolic problems can march in time in interior domains with a time step, Δt, limited only by domain-of-dependence constraints, $c\Delta t \lesssim \Delta x$, independent of the polynomial degree.
- The cell updates require no communication with neighboring cells, so high-order Hermite methods essentially maximize the computation-to-communication ratio.

✉ Thomas Hagstrom
thagstrom@smu.edu

Daniel Appelö
appelo@vt.edu

Yann-Meing Law
yann-meing.law@polymtl.ca

[1] Department of Mathematics, Virginia Tech, Blacksburg 24060, VA, USA

[2] Department of Mathematics, Southern Methodist University, Dallas 75275, TX, USA

[3] Department of Mathematics and Industrial Engineering, Polytechnique Montréal, Montréal QC H3C 3A7, Quebec, Canada

Examples of the application of Hermite methods in the hyperbolic case include the original dissipative formulation [7] as well as more recent energy-conserving forms [3, 19, 20], which treat the scalar wave equation and the first-order acoustic system. The method presented here generalizes the conservative Hermite method to the more complex dispersive Maxwell system. This generalization requires some additions to the algorithms to handle the dispersion models as well as substantial changes to the convergence analysis even in the dielectric case. We note that [3, 19, 20] also include implementations on GPUs where the localization of the cell updates can be exploited. Although not considered here, we expect that efficient GPU implementations of the proposed schemes are possible and we hope to explore them in the subsequent work.

Here we consider the general dispersive Maxwell system:

$$\epsilon\,(1+\mathcal{K}_e*)\,\frac{\partial E}{\partial t} = \nabla\times H,$$
$$\mu\,(1+\mathcal{K}_m*)\,\frac{\partial H}{\partial t} = -\nabla\times E.$$

We assume Lorentz models for the temporal convolutions; precisely, with s the Laplace transform variable dual to time,

$$\hat{\mathcal{K}}_e = \sum_{j=1}^{N_e} \frac{\omega_{e,j}^2}{s^2+\gamma_{e,j}s+\Omega_{e,j}^2},$$
$$\hat{\mathcal{K}}_m = \sum_{j=1}^{N_m} \frac{\omega_{m,j}^2}{s^2+\gamma_{m,j}s+\Omega_{m,j}^2}.$$

Here we include the frequency dependence not only of the permittivity but also of the permeability to account for simple homogenized models of metamaterials. Note that more general models, as discussed in [16], could also be treated, and applications to the nonlinear dispersive media have been completed and will appear in follow-up publications. As our focus here is on energy-conserving discretizations, we will consider cases where the dissipation can be neglected, $\gamma_{e,j}=\gamma_{m,j}=0$, where the Lorentz model reduces to a so-called Sellmeier model. We eliminate the convolutions by introducing additional fields K_j, L_j, R_j, and S_j to obtain

$$\frac{\partial E}{\partial t} = \frac{1}{\epsilon}\nabla\times H - \sum_{j=1}^{N_e}\omega_{e,j}^2 K_j, \tag{1}$$
$$\frac{\partial K_j}{\partial t} = -\gamma_{e,j}K_j - \Omega_{e,j}^2 L_j + E, \tag{2}$$
$$\frac{\partial H}{\partial t} = -\frac{1}{\mu}\nabla\times E - \sum_{j=1}^{N_m}\omega_{m,j}^2 R_j, \tag{3}$$
$$\frac{\partial R_j}{\partial t} = -\gamma_{m,j}R_j - \Omega_{m,j}^2 S_j + H, \tag{4}$$
$$\frac{\partial L_j}{\partial t} = K_j,\ \frac{\partial S_j}{\partial t} = R_j. \tag{5}$$

After rescaling the variables, we can rewrite (1)–(5) in the form

$$\frac{\partial V}{\partial t} = \sum_k A_k\frac{\partial W}{\partial x_k} + MW - \Gamma_V V, \tag{6}$$

$$\frac{\partial W}{\partial t} = \sum_k A_k^{\mathrm{T}} \frac{\partial V}{\partial x_k} - M^{\mathrm{T}} V - \Gamma_W W \tag{7}$$

with

$$V = \begin{pmatrix} \sqrt{\epsilon} E \\ \sqrt{\epsilon}\omega_{e,1}\Omega_{e,1} L_1 \\ \vdots \\ \sqrt{\epsilon}\omega_{e,N_e}\Omega_{e,N_e} L_{N_e} \\ \sqrt{\mu}\omega_{m,1} R_1 \\ \vdots \\ \sqrt{\mu}\omega_{m,N_m} R_{N_m} \end{pmatrix}, \quad W = \begin{pmatrix} \sqrt{\mu} H \\ \sqrt{\mu}\omega_{m,1}\Omega_{m,1} S_1 \\ \vdots \\ \sqrt{\mu}\omega_{m,N_m}\Omega_{m,N_m} S_{N_m} \\ \sqrt{\epsilon}\omega_{e,1} K_1 \\ \vdots \\ \sqrt{\epsilon}\omega_{e,N_e} K_{N_e} \end{pmatrix}. \tag{8}$$

Here, in a 3×3 block form, the skew-symmetric matrices A_k encode the curl operator

$$\sum_{k=1}^{3} A_k \frac{\partial}{\partial x_k} = c \begin{pmatrix} \nabla\times & 0 & 0 \\ 0 & 0 & 0 \\ 0 & 0 & 0 \end{pmatrix}, \quad c = (\epsilon\mu)^{-1/2},$$

M is given by

$$M = \begin{pmatrix} 0 & 0 & -\mathrm{diag}(\omega_{e,j}) \\ 0 & 0 & \mathrm{diag}(\Omega_{e,j}) \\ \mathrm{diag}(\omega_{m,j}) & -\mathrm{diag}(\Omega_{m,j}) & 0 \end{pmatrix},$$

and the dissipation matrices are nonnegative and diagonal,

$$\Gamma_V = \mathrm{diag}(0\,0\,\gamma_{m,j}), \quad \Gamma_W = \mathrm{diag}(0\,0\,\gamma_{e,j}).$$

Spatial derivatives are only applied to E and H, and the characteristic speeds are c, 0. We thus conclude that the domain-of-dependence, which is fundamental to the application of Hermite methods, is unaffected by the dispersive corrections. In addition, an energy given by $\|V\|^2_{\mathrm{L}^2} + \|W\|^2_{\mathrm{L}^2}$ is conserved or dissipated (modulo boundary contributions), and the number and type of admissible boundary conditions are the same as for Maxwell's equations in a simple dielectric.

We note that a number of alternative discretization schemes have been proposed to simulate Maxwell's equations in the linear dispersive media. For example, extensions of the Yee scheme are analyzed by Bokil and Gibson in [5]. Discontinuous Galerkin methods have been considered by a number of authors [10, 14, 17, 18] and edge elements are studied by Yang et al. [21]. Finite difference methods on overlapping meshes are analyzed and tested by Banks et al. in [4]. The potential advantage of the methods we propose in comparison with these alternatives is the possibility for efficient implementations of very high-order approximations as well as the minimal communication requirements during large time steps.

2 Conservative Hermite Discretization of the Dispersive Maxwell System

The essential ingredients of all Hermite methods are:

i. a cuboidal primal and dual grid,
ii. degrees-of-freedom defined by tensor-product Taylor polynomials at the cell vertices,

iii. cell polynomials constructed as tensor-product Hermite-Birkhoff interpolants of the vertex data,
iv. local (cell-wise) evolution to produce the updated degrees-of-freedom at dual cell nodes.

Our focus here is on energy-conserving methods exploiting the special structure of the Maxwell system. To that end, we assume that $\gamma_{e,j} = \gamma_{m,j} = 0$. In our subsequent discussion, we will indicate how the method can be modified to include dissipation. We note that the original dissipative Hermite method analyzed by Goodrich et al. [7] is directly applicable to the dispersive Maxwell system. In contrast with the scheme proposed here, in the dissipative method, all fields are defined on both the primal and dual grid and thus at every time step. The energy, as measured in the Hermite-Birkhoff semi-norm defined below, is then decreased by the interpolation process at each step. A comparison between the dissipative and nondissipative discretizations for the scalar wave equation is presented in [3]. As might be expected, there is an efficiency advantage with the conservative discretization only needing to evolve half as many variables per step, which is manifested in the numerical experiments as a reduction in solution time by almost a factor of two. In addition, in some cases, the exact energy conservation may be a desired feature. If dissipative models are used, however, the original method can be used at a higher order than the method proposed here due to time step restrictions associated with the multistep formula used to evolve the dissipative terms. We are assuming a uniform Cartesian mesh and piecewise uniform media. Methods for treating mapped grids to accommodate smooth boundaries are straightforward to implement and will be briefly discussed later on. We are also exploring the use of purely Cartesian meshes and embedded boundaries [8]. Denote the vertices on the primal cells by $(x_{1,j_1}, x_{2,j_2}, x_{3,j_3})$ and on the dual cells by $(x_{1,\hat{j}_1}, x_{2,\hat{j}_2}, x_{3,\hat{j}_3})$ with $\hat{j}_\ell = j_\ell + 1/2$. Lastly set $\Delta x_k = x_{k,j_k+1} - x_{k,j_k} = x_{k,\hat{j}_k+1} - x_{k,\hat{j}_k}$.

We define V and W at different time levels, $t_n = n\Delta t$, $t_{n+1/2} = (n+1/2)\Delta t$, and on different grids. Using the standard multi-index notation, we define the degrees-of-freedom to be

$$V^{\alpha,h}_{j_1,j_2,j_3}(t_n) \approx \frac{\Delta x^{|\alpha|}}{\alpha!} D^\alpha V(x_{1,j_1}, x_{2,j_2}, x_{3,j_3}, t_n), \tag{9}$$

$$W^{\alpha,h}_{\hat{j}_1,\hat{j}_2,\hat{j}_3}(t_{n+1/2}) \approx \frac{\Delta x^{|\alpha|}}{\alpha!} D^\alpha W(x_{1,\hat{j}_1}, x_{2,\hat{j}_2}, x_{3,\hat{j}_3}, t_{n+1/2}) \tag{10}$$

with

$$\alpha = (\alpha_1, \alpha_2, \alpha_3), \quad 0 \leqslant \alpha_j \leqslant m, \quad |\alpha| = \alpha_1 + \alpha_2 + \alpha_3.$$

To describe the numerical process assume, we know $V^{\alpha,h}_{j_1,j_2,j_3}(t_n)$ and $W^{\alpha,h}_{\hat{j}_1,\hat{j}_2,\hat{j}_3}(t_{n+1/2})$. Our goal is to update V. The first step is to compute the tensor-product Hermite-Birkhoff interpolant of the W data. Precisely, we determine the unique tensor-product vector-valued polynomial

$$\tilde{W}_{j_1,j_2,j_3}(x_1,x_2,x_3) = \sum_{k_1=0}^{2m+1}\sum_{k_2=0}^{2m+1}\sum_{k_3=0}^{2m+1} C_{k_1,k_2,k_3}(x_1 - x_{1,j_1})^{k_1}(x_2 - x_{2,j_2})^{k_2}(x_3 - x_{3,j_3})^{k_3}$$

satisfying the interpolation conditions

$$\frac{\Delta x^{|\alpha|}}{\alpha!} D^\alpha \tilde{W}_{j_1,j_2,j_3}(\mathbf{x}_{j_1\pm1/2,j_2\pm1/2,j_3\pm1/2}) = W^{\alpha,h}_{j_1\pm1/2,j_2\pm1/2,j_3\pm1/2}(t_{n+1/2}). \tag{11}$$

To evolve, we choose q and use the Taylor approximation

$$V(t_{n+1}) = V(t_n) + 2\sum_{\ell=1}^{q} \frac{(\Delta t/2)^{2\ell-1}}{(2\ell-1)!} \frac{\mathrm{d}^{2\ell-1}V}{\mathrm{d}t^{2\ell-1}}(t_{n+1/2}).$$

The time derivatives can be recursively computed using only $\tilde{W}$:

$$V^1 = \sum_k A_k \frac{\partial \tilde{W}_{j_1,j_2,j_3}}{\partial x_k} + M\tilde{W}_{j_1,j_2,j_3}, \tag{12}$$

$$V^\ell = \left(\sum_k A_k \frac{\partial}{\partial x_k} + M\right)\left(\sum_k A_k^{\mathrm{T}} \frac{\partial V^{\ell-1}}{\partial x_k} - M^{\mathrm{T}} V^{\ell-1}\right). \tag{13}$$

We emphasize that the functions V^ℓ are all tensor-product polynomials. Thus, the updated data can be obtained by simply differentiating the temporal Taylor series in space:

$$V^{\alpha,h}_{j_1,j_2,j_3}(t_{n+1}) = V^{\alpha,h}_{j_1,j_2,j_3}(t_n) + \frac{\Delta x^{|\alpha|}}{\alpha!} D^\alpha \left(2\sum_{\ell=1}^{q} \frac{(\Delta t/2)^{2\ell-1}}{(2\ell-1)!} V^\ell\right)(\mathbf{x}_{j_1,j_2,j_3}). \tag{14}$$

The procedure for updating W from $t_{n-1/2}$ to $t_{n+1/2}$ is completely analogous; we list the steps below for completeness. First, compute the interpolating polynomial $\tilde{V}_{\hat{j}_1,\hat{j}_2,\hat{j}_3}$ satisfying

$$\frac{\Delta x^{|\alpha|}}{\alpha!} D^\alpha \tilde{V}_{\hat{j}_1,\hat{j}_2,\hat{j}_3}(\mathbf{x}_{\hat{j}_1\pm 1/2,\hat{j}_2\pm 1/2,\hat{j}_3\pm 1/2}) = V^{\alpha,h}_{\hat{j}_1\pm 1/2,\hat{j}_2\pm 1/2,\hat{j}_3\pm 1/2}(t_n). \tag{15}$$

Then compute time derivatives recursively:

$$W^1 = \sum_k A_k^{\mathrm{T}} \frac{\partial \tilde{V}_{\hat{j}_1,\hat{j}_2,\hat{j}_3}}{\partial x_k} - M^{\mathrm{T}} \tilde{V}_{\hat{j}_1,\hat{j}_2,\hat{j}_3}, \tag{16}$$

$$W^\ell = \left(\sum_k A_k^{\mathrm{T}} \frac{\partial}{\partial x_k} - M^{\mathrm{T}}\right)\left(\sum_k A_k \frac{\partial W^{\ell-1}}{\partial x_k} + M W^{\ell-1}\right). \tag{17}$$

Finally, update the solution data:

$$W^{\alpha,h}_{\hat{j}_1,\hat{j}_2,\hat{j}_3}(t_{n+1/2}) = W^{\alpha,h}_{\hat{j}_1,\hat{j}_2,\hat{j}_3}(t_{n-1/2}) + \frac{\Delta x^{|\alpha|}}{\alpha!} D^\alpha \left(2\sum_{\ell=1}^{q} \frac{(\Delta t/2)^{2\ell-1}}{(2\ell-1)!} W^\ell\right)(\mathbf{x}_{\hat{j}_1,\hat{j}_2,\hat{j}_3}). \tag{18}$$

2.1 Dissipative Corrections

To include the dissipation terms in the evolution, we propose solving a differential equation for these terms using an implicit Nordsieck method in a predictor-corrector form as described by Byrne and Hindmarsh [6]; see also [8, Ch. III-6]. For example, consider corrections to (14). Define $\tilde{D}_V$ and $\tilde{D}_W$ as solutions to the differential equations:

$$\frac{\partial \tilde{D}_V}{\partial t} = -\Gamma_V V, \quad \frac{\partial \tilde{D}_W}{\partial t} = -\Gamma_W W. \tag{19}$$

Note that since the dissipation matrices are diagonal and equal to zero in many blocks, these equations do not involve all the variables. The degrees-of-freedom in the Nordsieck method

are the coefficients of a temporal Taylor polynomial scaled by the time step. Precisely, we have the space-time representations within a cell and at time levels t_n, $t_{n+1/2}$:

$$\tilde{D}_{V,j_1,j_2,j_3}(x_1,x_2,x_3,t) \approx \sum_{k=0}^{q_N} \tilde{D}_{V,j_1,j_2,j_3,k}(x_1,x_2,x_3)\frac{(t-t_n)^k}{\Delta t^k}, \tag{20}$$

$$\tilde{D}_{W,\hat{j}_1,\hat{j}_2,\hat{j}_3}(x_1,x_2,x_3,t) \approx \sum_{k=0}^{q_N} \tilde{D}_{W,\hat{j}_1,\hat{j}_2,\hat{j}_3,k}(x_1,x_2,x_3)\frac{(t-t_{n+1/2})^k}{\Delta t^k}, \tag{21}$$

where $\tilde{D}_{V,j_1,j_2,j_3,k}$ is a tensor-product polynomial in (x_1, x_2, x_3) represented as V in (9) and $\tilde{D}_{W,\hat{j}_1,\hat{j}_2,\hat{j}_3,k}$ is represented as W in (10). Then $\tilde{D}_{\tilde{W},j_1,j_2,j_3,k}$ is computed via the Hermite-Birkhoff spatial interpolation exactly as $\tilde{W}$, leading to

$$\tilde{D}_{\tilde{W},j_1,j_2,j_3}(x_1,x_2,x_3,t) \approx \sum_{k=0}^{q_N} \tilde{D}_{\tilde{W},j_1,j_2,j_3,k}(x_1,x_2,x_3)\frac{(t-t_{n+1/2})^k}{\Delta t^k}.$$

Maintaining the structure of (14), we must simply incorporate the additional terms in the formulas (12)–(13), evaluating all terms involving $\tilde{D}_{V,j_1,j_2,j_3}$ and $\tilde{D}_{\tilde{W},j_1,j_2,j_3}$ at $t_{n+1/2}$:

$$V^1 = \sum_k A_k \frac{\partial \tilde{W}_{j_1,j_2,j_3}}{\partial x_k} + M\tilde{W}_{j_1,j_2,j_3} + \frac{\partial \tilde{D}_{V,j_1,j_2,j_3}}{\partial t}, \tag{22}$$

$$\begin{aligned} V^\ell = &\left(\sum_k A_k \frac{\partial}{\partial x_k} + M\right)\left(\sum_k A_k^{\mathrm{T}} \frac{\partial V^{\ell-1}}{\partial x_k} - M^{\mathrm{T}} V^{\ell-1}\right) \\ &+ \frac{\partial^{2\ell-2}\tilde{D}_{\tilde{W},j_1,j_2,j_3}}{\partial t^{2\ell-2}} + \frac{\partial^{2\ell-1}\tilde{D}_{V,j_1,j_2,j_3}}{\partial t^{2\ell-1}}. \end{aligned} \tag{23}$$

Here we note that we are using the predicted values of $\tilde{D}_V$; that is the space-time polynomial centered at t_n. Since it is interpolated, the terms involving $\tilde{D}_{\tilde{W}}$ will have the tensor-product degree $2m+1$ while $\tilde{D}_V$ will only be of degree m. Due to the shrinking stability domain of the Nordsieck methods with increasing q_N, we limit the order used to represent the dissipative terms. Therefore, the formal temporal order of the method will now be less than the spatial order for large values of m.

We must also update the Taylor representation (20), enforcing (19) at t_{n+1} using the formulas derived by Byrne and Hindmarsh [6]. Coefficients of the predicted values of $\tilde{D}_{V,j_1,j_2,j_3}$ are simply obtained by recentering (20):

$$\sum_{k=0}^{q_N} \tilde{D}^{(p)}_{V,j_1,j_2,j_3,k}(x_1,x_2,x_3)\frac{(t-t_{n+1})^k}{\Delta t^k} = \sum_{k=0}^{q_N} \tilde{D}_{V,j_1,j_2,j_3,k}(x_1,x_2,x_3)\frac{(t-t_n)^k}{\Delta t^k}.$$

The updates are written in terms of coefficients ℓ_{j,q_N}, $j = 0, \cdots, q_N$, defined by

$$\sum_{j=0}^{q_N} \ell_{j,q_N} u^j = \frac{\int_{-1}^{u} \prod_{k=1}^{q_N-1}(s+k)\,\mathrm{d}s}{\int_{-1}^{0} \prod_{k=1}^{q_N-1}(s+k)\,\mathrm{d}s}.$$

Then, with all quantities representing spatial polynomials,

$$\delta = -\frac{1}{\ell_{1,q_N}}\left(\Delta t \Gamma_V V^1 + \tilde{D}^{(p)}_{V,j_1,j_2,j_3,1}\right),$$

$$\tilde{D}_{V,j_1,j_2,j_3,k} = \tilde{D}^{(p)}_{V,j_1,j_2,j_3,k} + \delta\ell_{k,q_N}.$$

The dissipative corrections at the other half-step are analogous with the roles of $\tilde{D}_V$ and $\tilde{D}_W$ reversed. That is, $\tilde{D}_{\tilde{V}}$ and $\tilde{D}_W$ appear in the formulas, and $\tilde{D}_W$ is updated using the predictor-corrector scheme.

We remark that the implicit assumption in this procedure is that the dissipative corrections are small. Then we expect that their inclusion will have a negligible effect on the time step stability constraints. Although we exclude these terms in our analysis we include them in one of the numerical examples. We then find that in some cases the order reduction is significant and hence sometimes favors the use of lower values of m than in the nondissipative cases.

2.2 Implementation in Mapped Coordinates and Compatibility Conditions

The methods we have proposed are most efficient for the piecewise uniform media. In particular, the recursions (12)–(13) and (16)–(17) require significantly fewer operations when no differentiations of the coefficients are needed. At boundaries and interfaces some modifications are required. As mentioned above, we are experimenting with the embedded boundary and interface methods. Although it is at this time unclear if that method can be extended to a high order, it should be possible to combine it with higher-order methods away from boundaries and interfaces. The alternative is to use mapped cells where necessary and to use the equations in conjunction with the interface conditions to extend the solution to ghost nodes. This approach is proposed by Loya et al. [13]. We note that one can choose to either define the component vectors in reference to a fixed Cartesian system or also transform them into components referenced to the mapped system as proposed for the Yee scheme in [9]. In either case, the only change to the method appears in the details of the recursions. As suggested in [13], using a representation of the mapping as a Taylor polynomial of a sufficiently high order centered in the cell, the additional cost involves the multiplication of the derivatives of the field interpolants by the coefficients arising from the mapping. For example,

$$\frac{\partial V}{\partial x_k} = \sum_j \frac{\partial r_j}{\partial x_k}\frac{\partial V}{\partial r_j},$$

increasing the cost due to the three polynomial multiplications. Note that these multiplications can be truncated according to the eventual truncation of the update.

The major complication in the implementation of Hermite methods is the imposition of the boundary and interface conditions. This stems from the need to provide the normal derivative data to update the solution in the cells adjacent to the boundary. For the dissipative formulation, three approaches have had success.

i. Coupling with discontinuous Galerkin discretizations in a possibly unstructured mesh near the boundary [1]. Here local time-stepping in the DG elements allows us to retain the large global time steps in most of the domain.
ii. The correction function method [12]. This involves a weighted least squares construction of a space-time polynomial near the boundary. Penalty terms in the least squares construction involve the boundary evolution, Maxwell's equations, and a match with the Hermite evolution in nearby volume cells.
iii. Compatibility conditions [13]. Here one uses the boundary conditions along with the equation and its normal and tangential derivatives to compute the missing data required to evolve the polynomial at the boundary.

Of these methods, only the compatibility approach has been demonstrated to work with a conservative Hermite method, namely the scheme for the scalar wave equation studied by Appelö et al. [3]. As such it is not directly applicable to the Maxwell system studied here though it is a promising avenue for future research to explore its extension to the present case. Consider the example of a flat PEC boundary $x_1 =$ constant. Then if the mesh containing the magnetic field is aligned with the boundary the problem is to determine the electric field and its derivatives at a dual ghost node. This is easily accomplished by assuming that the tangential fields are extended as odd functions and the normal field as an even function. Extending this procedure to a curved boundary and mapped coordinates leads to an algebraic system enforcing a zero tangential field along the boundary and a zero normal derivative of the projection of the electric field in the normal direction. In [13], the scalar wave equation is considered and the sixth-order convergence for a conservative Hermite scheme with $m = 3$ is demonstrated.

3 Stability and Convergence

To establish the stability and convergence of the proposed method, we exploit the projection property of the Hermite-Birkhoff interpolation process defined by (11) and (15) along with standard interpolation error estimates. (See [3, 7, 20] for detailed proofs.) We will assume throughout this section that the solution is 2π-periodic in each Cartesian coordinate and denote the domain by $\mathbb{T}$. Denote by $\mathcal{I}_m$ the interpolation operator; to cut down on the required notation, we use the same symbol for interpolation on the dual and primal grids. The essential property is expressed as the orthogonality of interpolants and interpolation errors in the semi-inner product (24), which we will call the HB inner product. Introducing the notation for the L^2 inner product of vector-valued functions

$$\langle u, v\rangle_{(L^2(\mathbb{T}))^3} = \int_{-\pi}^{\pi}\int_{-\pi}^{\pi}\int_{-\pi}^{\pi}\sum_{j=1}^{3} u_j(x_1,x_2,x_3)v_j(x_1,x_2,x_3)\mathrm{d}x_1\mathrm{d}x_2\mathrm{d}x_3,$$

we define for any vector functions f and g the semi-inner-product

$$\langle f, g\rangle_m = \left\langle \frac{\partial^{3m+3} f}{\partial x_1^{m+1}\partial x_2^{m+1}\partial x_3^{m+1}}, \frac{\partial^{3m+3} g}{\partial x_1^{m+1}\partial x_2^{m+1}\partial x_3^{m+1}} \right\rangle_{(L^2(\mathbb{T}))^3}. \tag{24}$$

Define the Hermite-Birkhoff interpolation operator $\mathcal{I}_m$ by setting $\mathcal{I}_m f$ for a periodic function f to be the periodic piecewise polynomial $\tilde{f}$ defined as in (11) or (15). (To keep the notation as simple as possible, we do not distinguish between the interpolation on the primal and dual grids.) Then we have

$$\langle \mathcal{I}_m f, g - \mathcal{I}_m g\rangle_m = 0. \tag{25}$$

Denoting by $|\cdot|_m^2$, the semi-norm associated with the semi-inner-product, (25) implies the Pythagorean Theorem:

$$|f|_m^2 = |\mathcal{I}_m f|_m^2 + |f - \mathcal{I}_m f|_m^2. \tag{26}$$

We will focus on establishing the stability and convergence for the case of a dielectric medium. That is, we set $M = \Gamma_V = \Gamma_W = 0$ and thus only need to evolve the electric and magnetic fields E and H. Since the dispersive terms present themselves as zero-order perturbations to the dielectric system, they are straightforward to include, at least suboptimally,

once the principal order terms have been handled. The analysis in the dielectric case consists of three main parts.

i. Using the Fourier series, we establish an exact conservation law for the Maxwell system staggered in time. This law holds in any Sobolev semi-norm, including the HB semi-norm defined above.
ii. Using the fact that the Hermite method can be written as an exact evolution followed by interpolation, we establish a discrete conservation law which is closely related to the exact conservation law for the continuous system restricted to the HB semi-norm. In particular, it differs only by terms arising from the interpolation error.
iii. Comparing the exact and discrete conservation laws we derive error estimates.

Lastly, we extend the analysis to dispersive models without dissipation using a more standard energy argument, but leveraging the stability analysis in the dielectric case.

3.1 Conserved Quantities for the Continuous Problem

Expanding in a Fourier series in space, let $\hat{E}(k,t)$, $\hat{H}(k,t)$ be the Fourier coefficients of the symmetrized variables $\tilde{E} = \sqrt{\epsilon}E$, $\tilde{H} = \sqrt{\mu}H$. They satisfy the ordinary differential equations

$$\frac{\partial \hat{E}}{\partial t} = \mathrm{i}ck \times \hat{H}, \quad \frac{\partial \hat{H}}{\partial t} = -\mathrm{i}ck \times \hat{E}. \tag{27}$$

For $k \neq 0$, set $k = |k|\hat{k}$. We will make use of an orthogonal decomposition of the fields $\tilde{E} = E_S + E_N$, $\tilde{H} = H_S + H_N$ defined for any vector function U by

$$\widehat{U_N}(k) = \hat{k}\hat{k}^{\mathrm{T}}\hat{U}(k), \quad \widehat{U_S}(k) = \hat{U}(k) - \widehat{U_N}(k). \tag{28}$$

We also define the operator $\mathcal{C}$ applied to any vector function U by

$$\widehat{\mathcal{C}U}(k) = \hat{k} \times \hat{U}(k), \tag{29}$$

and note the identities which follow from elementary identities satisfied by the cross-product

$$\mathcal{C}U = \mathcal{C}U_S, \quad \mathcal{C}^2 U_S = -U_S, \quad \left|\widehat{\mathcal{C}U_S}(k)\right| = \left|\widehat{U_S}(k)\right|. \tag{30}$$

The last identity combined with Parseval's relation implies that $\mathcal{C}$ preserves all Sobolev norms of U_S.

We also define operators $S^{\pm}$ as in [3, 20]:

$$\widehat{S^{\pm}U}(k) = \mathrm{e}^{\pm \mathrm{i}c|k|\Delta t/2}\hat{U}(k), \tag{31}$$

noting that $S^{-} = S^{+,*}$ and that the operators are unitary:

$$S^{+}S^{-} = S^{-}S^{+} = I. \tag{32}$$

In addition, they commute with the operator $\mathcal{C}$ and the orthogonal decomposition onto S and N vector components. Using these operators, we define the following functions:

$$\begin{aligned} P^{\pm}(\mathbf{x},t) &= E_S(\mathbf{x},t) \mp S^{\pm}\mathcal{C}H_S(\mathbf{x},t-\Delta t/2), \\ Q^{\pm}(\mathbf{x},t+\Delta t/2) &= H_S(\mathbf{x},t+\Delta t/2) \pm S^{\pm}\mathcal{C}E_S(\mathbf{x},t), \end{aligned} \tag{33}$$

and prove the following continuous conservation law.

Theorem 1 *For the dielectric system $M = \Gamma_V = \Gamma_W = 0$ and any Sobolev norm or semi-norm*

$$\|P^{\pm}(\cdot, t + \Delta t)\| = \|Q^{\pm}(\cdot, t + \Delta t/2)\| = \|P^{\pm}(\cdot, t)\|. \tag{34}$$

Proof Consider first the exact formula for the electric field:

$$\tilde{E}(\mathbf{x}, t + \Delta t) = \tilde{E}(\mathbf{x}, t) + 2\sum_{\ell=1}^{\infty}(-1)^{\ell-1}\frac{(\Delta t/2)^{2\ell-1}}{(2\ell-1)!}(\nabla\times)^{2\ell-1}\tilde{H}(\mathbf{x}, t + \Delta t/2).$$

In the Fourier space, we have

$$\begin{aligned}\hat{E}(\mathbf{k}, t + \Delta t) &= \hat{E}(\mathbf{k}, t) + 2\sum_{\ell=1}^{\infty}(-1)^{\ell-1}\frac{(\Delta t/2)^{2\ell-1}}{(2\ell-1)!}(\mathrm{i}ck\times)^{2\ell-1}\hat{H}(\mathbf{k}, t + \Delta t/2)\\ &= \hat{E}(\mathbf{k}, t) + 2\sum_{\ell=1}^{\infty}(-1)^{\ell-1}\frac{(\mathrm{i}c|k|\Delta t/2)^{2\ell-1}}{(2\ell-1)!}(\hat{k}\times)^{2\ell-1}\hat{H}(\mathbf{k}, t + \Delta t/2).\end{aligned}$$

Using $(\hat{k}\times)^{2\ell-1}\hat{H} = (-1)^{\ell-1}\hat{k}\times\hat{H}$ leads to

$$\begin{aligned}\hat{E}(\mathbf{k}, t + \Delta t) &= \hat{E}(\mathbf{k}, t) + \left(2\sum_{\ell=1}^{\infty}\frac{(\mathrm{i}c|k|\Delta t/2)^{2\ell-1}}{(2\ell-1)!}\right)\hat{k}\times\hat{H}(\mathbf{k}, t + \Delta t/2)\\ &= \hat{E}(\mathbf{k}, t) + \left(\mathrm{e}^{\mathrm{i}c|k|\Delta t/2} - \mathrm{e}^{-\mathrm{i}c|k|\Delta t/2}\right)\hat{k}\times\hat{H}(\mathbf{k}, t + \Delta t/2).\end{aligned}$$

Repeating a similar procedure for the magnetic field, the exact evolution formulas in terms of $\mathcal{C}$ and $S^{\pm}$ take the form:

$$\tilde{E}(\mathbf{x}, t + \Delta t) = \tilde{E}(\mathbf{x}, t) + \left(S^{+} - S^{-}\right)\mathcal{C}\tilde{H}(\mathbf{x}, t + \Delta t/2), \tag{35}$$

$$\tilde{H}(\mathbf{x}, t + \Delta t/2) = \tilde{H}(\mathbf{x}, t - \Delta t/2) - \left(S^{+} - S^{-}\right)\mathcal{C}\tilde{E}(\mathbf{x}, t). \tag{36}$$

Rewriting these in terms of the orthogonal decompositions (28) and utilizing (30), we have

$$E_S(\mathbf{x}, t + \Delta t) = E_S(\mathbf{x}, t) + \left(S^{+} - S^{-}\right)\mathcal{C}H_S(\mathbf{x}, t + \Delta t/2), \tag{37}$$

$$H_S(\mathbf{x}, t + \Delta t/2) = H_S(\mathbf{x}, t - \Delta t/2) - \left(S^{+} - S^{-}\right)\mathcal{C}E_S(\mathbf{x}, t), \tag{38}$$

$$E_N(\mathbf{x}, t + \Delta t) = E_N(\mathbf{x}, t), \tag{39}$$

$$H_N(\mathbf{x}, t + \Delta t/2) = H_N(\mathbf{x}, t - \Delta t/2). \tag{40}$$

Assuming $\nabla\cdot E = \nabla\cdot H = 0$ initially, (39)–(40) simply imply that the fields will be solenoidal at all subsequent discrete times. (We will assume this to be true when estimating the errors.) Again using (30) and (32), we rewrite the evolution formulas (37)–(38):

$$\begin{cases} P^+(\mathbf{x}, t+\Delta t) = -S^-\mathcal{C}Q^+(\mathbf{x}, t+\Delta t/2), \\ P^-(\mathbf{x}, t+\Delta t) = S^+\mathcal{C}Q^-(\mathbf{x}, t+\Delta t/2), \\ Q^+(\mathbf{x}, t+\Delta t/2) = S^-\mathcal{C}P^+(\mathbf{x}, t), \\ Q^-(\mathbf{x}, t+\Delta t/2) = -S^+\mathcal{C}P^-(\mathbf{x}, t). \end{cases} \tag{41}$$

Equation (34) then follows due to the norm preserving properties of the operators $S^{\pm}$ and $\mathcal{C}$.

3.2 Conserved Quantities for the Discrete Problem

We now note that for polynomial data the recursions (13) and (17) will terminate once the number of spatial derivatives exceeds the degree. For the tensor-product polynomials of the total degree $6m+3$, we have

$$V_\ell = W_\ell = 0, \quad \ell > 3m+2.$$

Thus, if we take $q = 3m+2$ the cell polynomials are evolved exactly. Moreover, if we obey the CFL restriction

$$c\Delta t < \max_k \Delta x_k, \tag{42}$$

then we have the following lemma. Here we define $\tilde{E}^h$, $\tilde{H}^h$ to be the Hermite-Birkhoff interpolants of the vertex data and define the quantities $P^{\pm,h}$, $Q^{\pm,h}$ as in (33).

Lemma 1 *For the dielectric system $M = \Gamma_V = \Gamma_W = 0$, if $q = 3m+2$ and (42) holds, then the quantities $P^{\pm,h}$, E_N^h, $Q^{\pm,h}$, and H_N^h computed from the approximations, $\tilde{E}^h$, $\tilde{H}^h$, to the symmetrized variables satisfy the evolution formulas*:

$$\begin{cases} P^{+,h}(\mathbf{x}, t+\Delta t) + E_N^h(\mathbf{x}, t+\Delta t) \\ = -\mathcal{I}_m\left(S^-\mathcal{C}Q^{+,h}(\mathbf{x}, t+\Delta t/2) - E_N^h(\mathbf{x}, t)\right) \\ \quad -(1-\mathcal{I}_m)\left(S^+\mathcal{C}Q^{-,h}(\mathbf{x}, t+\Delta t/2) + E_N^h(\mathbf{x}, t)\right), \\ P^{-,h}(\mathbf{x}, t+\Delta t) + E_N^h(\mathbf{x}, t+\Delta t) \\ = \mathcal{I}_m\left(S^+\mathcal{C}Q^{-,h}(\mathbf{x}, t+\Delta t/2) + E_N^h(\mathbf{x}, t)\right) \\ \quad +(1-\mathcal{I}_m)\left(S^-\mathcal{C}Q^{+,h}(\mathbf{x}, t+\Delta t/2) - E_N^h(\mathbf{x}, t)\right), \\ Q^{+,h}(\mathbf{x}, t+\Delta t/2) + H_N^h(\mathbf{x}, t+\Delta t/2) \\ = \mathcal{I}_m\left(S^-\mathcal{C}P^{+,h}(\mathbf{x}, t) + H_N^h(\mathbf{x}, t-\Delta t/2)\right) \\ \quad +(1-\mathcal{I}_m)\left(S^+\mathcal{C}P^{-,h}(\mathbf{x}, t) - H_N^h(\mathbf{x}, t-\Delta t/2)\right), \\ Q^{-,h}(\mathbf{x}, t+\Delta t/2) + H_N^h(\mathbf{x}, t+\Delta t/2) \\ = -\mathcal{I}_m\left(S^+\mathcal{C}P^{-,h}(\mathbf{x}, t) - H_N^h(\mathbf{x}, t-\Delta t/2)\right) \\ \quad -(1-\mathcal{I}_m)\left(S^-\mathcal{C}P^{+,h}(\mathbf{x}, t) + H_N^h(\mathbf{x}, t-\Delta t/2)\right). \end{cases} \tag{43}$$

Proof Assuming (42), the domain of dependence of the solution at the cell centers on either grid lies completely within the cell. Therefore, since the cell polynomial is updated exactly

if we take $q = 3m + 2$, the data used to compute the Hermite-Birkhoff interpolants is the exact evolution of the approximate solution at the previous times. Thus, the only error over a time step is the interpolation error which can then be projected onto the various solution components. The further complications in (43) in comparison to (41) arise from the fact that the projections do not commute with $\mathcal{I}_m$. Recalling that $\mathcal{I}_m$ is a projection the discrete evolution formulas are

$$\tilde{E}^h(\mathbf{x}, t + \Delta t) = \tilde{E}^h(\mathbf{x}, t) + \mathcal{I}_m \left(S^+ - S^-\right) \mathcal{C} H_S^h(\mathbf{x}, t + \Delta t/2), \tag{44}$$

$$\tilde{H}^h(\mathbf{x}, t + \Delta t/2) = \tilde{H}^h(\mathbf{x}, t - \Delta t/2) - \mathcal{I}_m \left(S^+ - S^-\right) \mathcal{C} E_S^h(\mathbf{x}, t). \tag{45}$$

Consider, for example, the updated formula for $P^{+,h} + E_N^h$ making use of (44)–(45) along with (30) and (32). Note that

$$\begin{aligned} \tilde{E}^h(\mathbf{x}, t) &= \mathcal{I}_m \tilde{E}^h(\mathbf{x}, t) = -\mathcal{I}_m S^- \mathcal{C} S^+ \mathcal{C} E_S^h(\mathbf{x}, t) + \mathcal{I}_m E_N^h(\mathbf{x}, t), \\ 0 &= -(1 - \mathcal{I}_m)\tilde{E}^h(\mathbf{x}, t) = (1 - \mathcal{I}_m) S^+ \mathcal{C} S^- \mathcal{C} E_S^h(\mathbf{x}, t) - (1 - \mathcal{I}_m) E_N^h(\mathbf{x}, t). \end{aligned}$$

We compute

$$\begin{aligned} & P^{+,h}(\mathbf{x}, t + \Delta t) + E_N^h(\mathbf{x}, t + \Delta t) \\ &= \tilde{E}^h(\mathbf{x}, t + \Delta t) - S^+ \mathcal{C} H_S^h(\mathbf{x}, t + \Delta t/2) \\ &= -\mathcal{I}_m \left(S^- \mathcal{C} \left(H_S^h(\mathbf{x}, t + \Delta t/2) + S^+ \mathcal{C} E_S^h(\mathbf{x}, t) \right) - E_N^h(\mathbf{x}, t) \right) \\ &= -(1 - \mathcal{I}_m) \left(S^+ \mathcal{C} \left(H_S^h(\mathbf{x}, t + \Delta t/2) - S^- \mathcal{C} E_S^h(\mathbf{x}, t) \right) + E_N^h(\mathbf{x}, t) \right) \\ &= -\mathcal{I}_m \left(S^- \mathcal{C} Q^{+,h}(\mathbf{x}, t + \Delta t/2) - E_N^h(\mathbf{x}, t) \right) \\ &\quad -(1 - \mathcal{I}_m) \left(S^+ \mathcal{C} Q^{-,h}(\mathbf{x}, t + \Delta t/2) + E_N^h(\mathbf{x}, t) \right). \end{aligned}$$

The other identities in (43) are similarly derived.

We are now in a position to prove Theorem 2, the discrete analog of Theorem 1.

Theorem 2 *For the dielectric system $M = \Gamma_V = \Gamma_W = 0$, if $q = 3m + 2$ and (42) holds, then the approximate solution satisfies the conservation laws*

$$\begin{aligned} & \left| P^{+,h}(\cdot, t + \Delta t) \right|_m^2 + \left| P^{-,h}(\cdot, t + \Delta t) \right|_m^2 \\ & +2 \left| E_N^h(\cdot, t + \Delta t) \right|_m^2 + 2 \left| H_N^h(\cdot, t + \Delta t/2) \right|_m^2 \\ &= \left| Q^{+,h}(\cdot, t + \Delta t/2) \right|_m^2 + \left| Q^{-,h}(\cdot, t + \Delta t/2) \right|_m^2 \\ & +2 \left| H_N^h(\cdot, t + \Delta t/2) \right|_m^2 + 2 \left| E_N^h(\cdot, t) \right|_m^2 \\ &= \left| P^{+,h}(\cdot, t) \right|_m^2 + \left| P^{-,h}(\cdot, t) \right|_m^2 + 2 \left| E_N^h(\cdot, t) \right|_m^2 + 2 \left| H_N^h(\cdot, t - \Delta t/2) \right|_m^2. \end{aligned} \tag{46}$$

Proof Compute recalling the fact that $P^{\pm,h}$, $Q^{\pm,h}$ and any other function in the range of $\mathcal{C}$ are orthogonal to E_N^h and H_N^h in the HB semi-inner product,

$$\left| P^{+,h}(\cdot, t + \Delta t) \right|_m^2 + \left| E_N^h(\cdot, t + \Delta t) \right|_m^2$$

$$
\begin{aligned}
&= \left| P^{+,h}(\cdot, t+\Delta t) + E_N^h(\cdot, t+\Delta t) \right|_m^2 \\
&= \left| \mathcal{I}_m \left(S^- \mathcal{C} Q^{+,h}(\cdot, t+\Delta t/2) - E_N^h(\cdot, t) \right) \right|_m^2 \\
&\quad + \left| (1-\mathcal{I}_m) \left(S^+ \mathcal{C} Q^{-,h}(\cdot, t+\Delta t/2) + E_N^h(\cdot, t) \right) \right|_m^2 \\
&= \left| \mathcal{I}_m S^- \mathcal{C} Q^{+,h}(\cdot, t+\Delta t/2) \right|_m^2 \\
&\quad + \left| (1-\mathcal{I}_m) S^+ \mathcal{C} Q^{-,h}(\cdot, t+\Delta t/2) \right|_m^2 + \left| E_N^h(\cdot, t) \right|_m^2 \\
&\quad - 2\langle \mathcal{I}_m S^- \mathcal{C} Q^{+,h}(\cdot, t+\Delta t/2), \mathcal{I}_m E_N^h(\cdot, t) \rangle_m \\
&\quad + 2\langle (1-\mathcal{I}_m) S^+ \mathcal{C} Q^{-,h}(\cdot, t+\Delta t/2), (1-\mathcal{I}_m) E_N^h(\cdot, t) \rangle_m, \\
&\quad \left| P^{-,h}(\cdot, t+\Delta t) \right|_m^2 + \left| E_N^h(\cdot, t+\Delta t) \right|_m^2 \\
&= \left| P^{-,h}(\cdot, t+\Delta t) + E_N^h(\cdot, t+\Delta t) \right|_m^2 \\
&= \left| \mathcal{I}_m \left(S^+ \mathcal{C} Q^{-,h}(\cdot, t+\Delta t/2) + E_N^h(\cdot, t) \right) \right|_m^2 \\
&\quad + \left| (1-\mathcal{I}_m) \left(S^- \mathcal{C} Q^{+,h}(\cdot, t+\Delta t/2) - E_N^h(\cdot, t) \right) \right|_m^2 \\
&= \left| \mathcal{I}_m S^+ \mathcal{C} Q^{-,h}(\cdot, t+\Delta t/2) \right|_m^2 \\
&\quad + \left| (1-\mathcal{I}_m) S^- \mathcal{C} Q^{+,h}(\cdot, t+\Delta t/2) \right|_m^2 + \left| E_N^h(\cdot, t) \right|_m^2 \\
&\quad + 2\langle \mathcal{I}_m S^+ \mathcal{C} Q^{-,h}(\cdot, t+\Delta t/2), \mathcal{I}_m E_N^h(\cdot, t) \rangle_m \\
&\quad - 2\langle (1-\mathcal{I}_m) S^- \mathcal{C} Q^{+,h}(\cdot, t+\Delta t/2), (1-\mathcal{I}_m) E_N^h(\cdot, t) \rangle_m .
\end{aligned}
$$

Adding these expressions we find

$$
\begin{aligned}
&\left| P^{+,h}(\cdot, t+\Delta t) \right|_m^2 + \left| P^{-,h}(\cdot, t+\Delta t) \right|_m^2 + 2 \left| E_N^h(\cdot, t+\Delta t) \right|_m^2 \\
&= \left| S^- \mathcal{C} Q^{+,h}(\cdot, t+\Delta t/2) \right|_m^2 + \left| S^+ \mathcal{C} Q^{-,h}(\cdot, t+\Delta t/2) \right|_m^2 + 2 \left| E_N^h(\cdot, t) \right|_m^2 \\
&\quad - 2\langle \mathcal{I}_m S^- \mathcal{C} Q^{+,h}(\cdot, t+\Delta t/2), \mathcal{I}_m E_N^h(\cdot, t) \rangle_m \\
&\quad - 2\langle (1-\mathcal{I}_m) S^- \mathcal{C} Q^{+,h}(\cdot, t+\Delta t/2), (1-\mathcal{I}_m) E_N^h(\cdot, t) \rangle_m \\
&\quad + 2\langle (1-\mathcal{I}_m) S^+ \mathcal{C} Q^{-,h}(\cdot, t+\Delta t/2), (1-\mathcal{I}_m) E_N^h(\cdot, t) \rangle_m \\
&\quad + 2\langle \mathcal{I}_m S^+ \mathcal{C} Q^{-,h}(\cdot, t+\Delta t/2), \mathcal{I}_m E_N^h(\cdot, t) \rangle_m \\
&= \left| S^- \mathcal{C} Q^{+,h}(\cdot, t+\Delta t/2) \right|_m^2 + \left| S^+ \mathcal{C} Q^{-,h}(\cdot, t+\Delta t/2) \right|_m^2 + 2 \left| E_N^h(\cdot, t) \right|_m^2 \\
&\quad - 2\langle S^- \mathcal{C} Q^{+,h}(\cdot, t+\Delta t/2), E_N^h(\cdot, t) \rangle_m \\
&\quad + 2\langle S^+ \mathcal{C} Q^{-,h}(\cdot, t+\Delta t/2), E_N^h(\cdot, t) \rangle_m \\
&= \left| Q^{+,h}(\cdot, t+\Delta t/2) \right|_m^2 + \left| Q^{-,h}(\cdot, t+\Delta t/2) \right|_m^2 + 2 \left| E_N^h(\cdot, t) \right|_m^2 .
\end{aligned}
$$

Adding $2\left|H_N^h(\cdot, t+\Delta t/2)\right|_m^2$ to both sides of this equation yields the first equality in (46). The second is proven similarly using the updated formulas for $Q^{\pm,h}$ in (43).

It is useful to organize the previous results in terms of the evolution of the conserved quantities. Specifically, we introduce the HB semi-norm conserving operators $\mathcal{U}$ and $\mathcal{V}$:

$$\begin{pmatrix} P^{+,h}(\mathbf{x}, t+\Delta t) \\ P^{-,h}(\mathbf{x}, t+\Delta t) \\ E_N^h(\mathbf{x}, t+\Delta t) \\ H_N^h(\mathbf{x}, t+\Delta t/2) \end{pmatrix} = \mathcal{U}^h \begin{pmatrix} Q^{+,h}(\mathbf{x}, t+\Delta t/2) \\ Q^{-,h}(\mathbf{x}, t+\Delta t/2) \\ H_N^h(\mathbf{x}, t+\Delta t/2) \\ E_N^h(\mathbf{x}, t) \end{pmatrix}, \tag{47}$$

$$\begin{pmatrix} Q^{+,h}(\mathbf{x}, t+\Delta t/2) \\ Q^{-,h}(\mathbf{x}, t+\Delta t/2) \\ H_N^h(\mathbf{x}, t+\Delta t/2) \\ E_N^h(\mathbf{x}, t) \end{pmatrix} = \mathcal{V}^h \begin{pmatrix} P^{+,h}(\mathbf{x}, t) \\ P^{-,h}(\mathbf{x}, t) \\ E_N^h(\mathbf{x}, t) \\ H_N^h(\mathbf{x}, t-\Delta t/2) \end{pmatrix}. \tag{48}$$

3.3 Convergence

By comparing the evolution of the continuous and discrete conserved variables, we can finally derive an error estimate. Define errors in the conserved quantities by

$$\mathcal{E}(t_n) = \begin{pmatrix} P^+(\mathbf{x}, t_n) - P^{+,h}(\mathbf{x}, t_n) \\ P^-(\mathbf{x}, t_n) - P^{-,h}(\mathbf{x}, t_n) \\ E_N(\mathbf{x}, t_n) - E_N^h(\mathbf{x}, t_n) \\ H_N(\mathbf{x}, t_{n-1/2}) - H_N^h(\mathbf{x}, t_{n-1/2}) \end{pmatrix}, \tag{49}$$

$$\mathcal{E}(t_{n+1/2}) = \begin{pmatrix} Q^+(\mathbf{x}, t_{n+1/2}) - Q^{+,h}(\mathbf{x}, t_{n+1/2}) \\ Q^-(\mathbf{x}, t_{n+1/2}) - P^{-,h}(\mathbf{x}, t_{n+1/2}) \\ H_N(\mathbf{x}, t_{n+1/2}) - H_N^h(\mathbf{x}, t_{n+1/2}) \\ E_N(\mathbf{x}, t_n) - E_N^h(\mathbf{x}, t_n) \end{pmatrix}, \tag{50}$$

where we have introduced $t_n = n\Delta t$, $t_{n+1/2} = (n+1/2)\Delta t$. Convergence in the HB semi-norm is established in Theorem 3.

Theorem 3 *For the dielectric system $M = \Gamma_V = \Gamma_W = 0$, if $q = 3m+2$, the CFL number $\frac{\Delta t}{h}$ is fixed and satisfies (42), and the initial approximations are sufficiently accurate, then there exists C depending only on m, the CFL number, and derivatives of the solution $\tilde{E}(\mathbf{x}, t)$, $\tilde{H}(\mathbf{x}, t)$, such that, for $h = \max(h_x, h_y, h_z)$,*

$$|\mathcal{E}(t_n)|_m + \left|\mathcal{E}(t_{n+1/2})\right|_m \leqslant C\,(1+t_n)\,h^m. \tag{51}$$

Proof We combine (43) with the exact formulas (37)–(40) to derive evolution formulas for $\mathcal{E}$. We begin with the first two equations. Note that we are assuming $E_N = 0$ and $H_N = 0$, but for clarity, we retain them in the error equations:

$$\begin{aligned}
&P^+(\mathbf{x}, t_{n+1}) - P^{+,h}(\mathbf{x}, t_{n+1}) + E_N(\mathbf{x}, t_{n+1}) - E_N^h(\mathbf{x}, t_{n+1}) \\
&= -\mathcal{I}_m \left(S^- \mathcal{C} \left(Q^+(\mathbf{x}, t_{n+1/2}) - Q^{+,h}(\mathbf{x}, t_{n+1/2}) \right) - \left(E_N(\mathbf{x}, t_n) - E_N^h(\mathbf{x}, t_n) \right) \right) \\
&\quad -(1-\mathcal{I}_m) \left(S^+ \mathcal{C} \left(Q^-(\mathbf{x}, t_{n+1/2}) - Q^{-,h}(\mathbf{x}, t_{n+1/2}) \right) + \left(E_N(\mathbf{x}, t_n) - E_N^h(\mathbf{x}, t_n) \right) \right) \\
&\quad +(1-\mathcal{I}_m) \left(S^+ \mathcal{C} Q^-(\mathbf{x}, t_{n+1/2}) - S^- \mathcal{C} Q^+(\mathbf{x}, t_{n+1/2}) \right), \\
&P^-(\mathbf{x}, t_{n+1}) - P^{-,h}(\mathbf{x}, t_n) + E_N(\mathbf{x}, t_{n+1}) - E_N^h(\mathbf{x}, t_{n+1}) \\
&= +\mathcal{I}_m \left(S^+ \mathcal{C} \left(Q^-(\mathbf{x}, t_{n+1/2}) - Q^{-,h}(\mathbf{x}, t_{n+1/2}) \right) + \left(E_N(\mathbf{x}, t_n) - E_N^h(\mathbf{x}, t_n) \right) \right)
\end{aligned}$$

$$+(1-\mathcal{I}_m)\left(S^-\mathcal{C}\left(Q^+(\mathbf{x},t_{n+1/2})-Q^{+,h}(\mathbf{x},t_{n+1/2})\right)-\left(E_N(\mathbf{x},t_n)-E_N^h(\mathbf{x},t_n)\right)\right)$$
$$+(1-\mathcal{I}_m)\left(S^+\mathcal{C}Q^-(\mathbf{x},t_{n+1/2})-S^-\mathcal{C}Q^+(\mathbf{x},t_{n+1/2})\right).$$

Similarly, we can write down the evolution of the error for E_N:

$$\begin{aligned}E_N(\mathbf{x},t_{n+1})-E_N^h(\mathbf{x},t_{n+1}) &= E_N(\mathbf{x},t_n)-E_N^h(\mathbf{x},t_n)\\ &\quad +N\mathcal{I}_m\left(S^+-S^-\right)\mathcal{C}\left(H_S(\mathbf{x},t_{n+1/2})-H_S^h(\mathbf{x},t_{n+1/2})\right)\\ &\quad +N(1-\mathcal{I}_m)\left(E_S(\mathbf{x},t_{n+1})-E_S(\mathbf{x},t_n)\right),\end{aligned}$$

where N is the projection operator defined in the Fourier space by the leftmost relation in (28). Note that the H_N error is simply copied in this step of the evolution. Noting that

$$\begin{aligned}&(1-\mathcal{I}_m)\left(S^+\mathcal{C}Q^-(\mathbf{x},t_{n+1/2})-S^-\mathcal{C}Q^+(\mathbf{x},t_{n+1/2})\right)\\ &=(1-\mathcal{I}_m)\left(P^+(\mathbf{x},t_{n+1})+P^-(\mathbf{x},t_{n+1})\right)\\ &=(1-\mathcal{I}_m)\left(E_S(\mathbf{x},t_{n+1})+E_S(\mathbf{x},t_n)\right),\end{aligned}$$

we can rewrite these relations as

$$\mathcal{E}(t_{n+1})=\mathcal{U}^h\mathcal{E}(t_{n+1/2})+\tau_{n+1},$$

where

$$\tau_{n+1}=\begin{pmatrix}\left[(1-\mathcal{I}_m)\left(E_S(\mathbf{x},t_{n+1})+E_S(\mathbf{x},t_n)\right)\right]_S\\ \left[(1-\mathcal{I}_m)\left(E_S(\mathbf{x},t_{n+1})+E_S(\mathbf{x},t_n)\right)\right]_S\\ \left[(1-\mathcal{I}_m)\left(E_S(\mathbf{x},t_{n+1})-E_S(\mathbf{x},t_n)\right)\right]_N\\ 0\end{pmatrix}.$$

Assuming a smooth solution to the continuous problem and a fixed CFL number, the standard Hermite-Birkhoff interpolation error formulas (e.g., [7]) imply

$$\left|(1-\mathcal{I}_m)\left(E_S(\mathbf{x},t_{n+1})+E_S(\mathbf{x},t_n)\right)\right|_m\leqslant C\frac{\Delta t}{2}h^m.$$

So invoking the triangle inequality for the semi-norm and the fact that $\mathcal{U}^h$ preserves the semi-norm we have

$$|\mathcal{E}(t_{n+1})|_m\leqslant\left|\mathcal{U}^h\mathcal{E}(t_{n+1/2})\right|_m+|\tau_{n+1}|_m\leqslant\left|\mathcal{E}(t_{n+1/2})\right|_m+C\frac{\Delta t}{2}h^m.$$

By similar computations, we deduce

$$\left|\mathcal{E}(t_{n+1/2})\right|_m\leqslant|\mathcal{E}(t_n)|_m+C\frac{\Delta t}{2}h^m.$$

Summing these inequalities, we have

$$|\mathcal{E}(t_n)|_m+\left|\mathcal{E}(t_{n+1/2})\right|_m\leqslant|\mathcal{E}(t_0)|_m+\left|\mathcal{E}(t_{1/2})\right|_m+Ct_nh^m.$$

Assuming, as would be the case if we interpolate a smooth initial condition and an initial half-step,

$$|\mathcal{E}(t_0)|_m\leqslant Ch^{m+1},\quad\left|\mathcal{E}(t_{1/2})\right|_m\leqslant Ch^{m+1},$$

we obtain the final result.

3.4 Extensions to the Dispersive System

The inclusion of the dispersive terms does not change the domain-of-dependence of the exact solution. Thus, excluding the dissipative terms, we believe that the previous analysis could be repeated via the definition of the complex exponentials of the operators appearing in the updated formulas. However, we can no longer expect to evolve the cell polynomials exactly and so need to take account of additional sources of error. Therefore, we will follow the standard analysis of stability for leap-frog schemes as presented in Joly [11]. Again ignoring the dissipative term and using the fact that $\mathcal{I}_m$ is a projection we can write the discrete evolution equations (14) and (18), in the form:

$$\begin{aligned} V(\mathbf{x}, t_{n+1}) - V(\mathbf{x}, t_n) &= \mathcal{I}_m \mathcal{B} \mathcal{I}_m W(\mathbf{x}, t_{n+1/2}), \\ W(\mathbf{x}, t_{n+1/2}) - W(\mathbf{x}, t_{n-1/2}) &= -\mathcal{I}_m \mathcal{B}^* \mathcal{I}_m V(\mathbf{x}, t_n), \end{aligned}$$

where

$$\mathcal{B}\mathcal{I}_m W = \sum_{\ell=1}^{q} \frac{(\Delta t/2)^{2\ell-1}}{(2\ell-1)!} V^{\ell} \tag{52}$$

with V^{ℓ} defined by (12)–(13). Now consider the scaling of terms in (12)–(13). When restricted to the polynomial space the derivative operators $\frac{\partial}{\partial x_k} \propto \Delta x_k^{-1}$. Therefore, for fixed CFL numbers, $\lambda_k = c\Delta t/\Delta x_k$, we have

$$\mathcal{I}_m \mathcal{B} \mathcal{I}_m = \mathcal{I}_m \left(\mathcal{B}_0 + \Delta t \mathcal{B}_1\right) \mathcal{I}_m, \tag{53}$$

where $\mathcal{B}_0$ is independent of Δt and $\mathcal{B}_1$ is bounded. In particular $\mathcal{B}_0$ is the evolution operator for the dielectric case combined with some additional zero blocks.

We then have Theorem 4 and the conditional stability follows.

Theorem 4 *For the conservative system $\Gamma_V = \Gamma_W = 0$, the following quantities are constant*:

$$|V(\cdot, t_n)|_m^2 + \frac{1}{4} \left|W(\cdot, t_{n+1/2}) + W(\cdot, t_{n-1/2})\right|_m^2 - \frac{1}{4} \left|\mathcal{I}_m B^* V(\cdot, t_n)\right|_m^2, \tag{54}$$

$$\left|W(\cdot, t_{n+1/2})\right|_m^2 + \frac{1}{4} |V(\cdot, t_{n+1}) + V(\cdot, t_n)|_m^2 - \frac{1}{4} \left|\mathcal{I}_m B^* W(\cdot, t_{n+1/2})\right|_m^2. \tag{55}$$

Corollary 1 *For the conservative system $\Gamma_V = \Gamma_W = 0$, we have the stability in the HB semi-norm if*

$$\|\mathcal{B}\|_m < 4, \quad \|\mathcal{B}^*\|_m < 4. \tag{56}$$

Remark 1 Condition (56) plays the role of a CFL condition. Invoking (53) and Theorem 2 and taking $q = 3m + 2$, we expect the stability for Δt small enough under the domain-of-dependence CFL condition (42). In our experiments, we find that the method is stable in both the dielectric and dispersive cases with large CFL numbers and smaller values of q.

Proof Combining two steps in (18), we have the formula

$$W(\mathbf{x}, t_{n+3/2}) - W(\mathbf{x}, t_{n-1/2}) = -\mathcal{I}_m \mathcal{B}^* \mathcal{I}_m \left(V(\mathbf{x}, t_{n+1}) + V(\mathbf{x}, t_n)\right).$$

Taking the HB inner product of this equation with $W(\mathbf{x}, t_{n+3/2})$ and the HB inner product of (14) with $V(\mathbf{x}, t_{n+1}) + V(\mathbf{x}, t_n)$, we obtain

$$\langle W(\cdot, t_{n+3/2}), W(\cdot, t_{n+1/2})\rangle_m = \langle W(\cdot, t_{n+1/2}), W(\cdot, t_{n-1/2})\rangle_m$$

$$-\langle W(\cdot, t_{n+1/2}), \mathcal{I}_m \mathcal{B}^* \mathcal{I}_m \left(V(\cdot, t_{n+1}) + V(\cdot, t_n)\right)\rangle_m,$$
$$|V(\cdot, t_{n+1})|_m^2 = |V(\cdot, t_n)|_m^2 + \langle \mathcal{I}_m \mathcal{B} \mathcal{I}_m W(\cdot, t_{n+1/2}), V(\cdot, t_{n+1}) + V(\cdot, t_n)\rangle_m.$$

Adding these expressions and noting that the terms involving $\mathcal{B}$ and $\mathcal{B}^*$ cancel, we deduce that the quantity

$$|V(\cdot, t_n)|_m^2 + \langle W(\cdot, t_{n+1/2}), W(\cdot, t_{n-1/2})\rangle_m$$

is constant. We rewrite the second term by noting that

$$\frac{1}{4}\left|W(\cdot, t_{n+1/2}) + W(\cdot, t_{n-1/2})\right|_m^2 - \frac{1}{4}\left|W(\cdot, t_{n+1/2}) - W(\cdot, t_{n-1/2})\right|_m^2$$
$$= \langle W(\cdot, t_{n+1/2}), W(\cdot, t_{n-1/2})\rangle_m.$$

Replacing the difference term with (18) yields (54). Equation (55) is derived by the analogous procedure.

Given the stability theorem, error estimates in the HB semi-norm can also be obtained by standard means. We will not present them here but instead focus on observing stability bounds and convergence rates in L^2 in numerical experiments. One can attempt a standard analysis of convergence by studying the local truncation error method and the associated stability of the scheme. The approximation of derivatives by the Hermite interpolant of a smooth function at the cell centers will have errors which scale with $|\Delta x|^{2m+2-j}$ for derivatives of the even order and $|\Delta x|^{2m+3-j}$ for derivatives of the odd order. Therefore, if we consider the evolution of the scaled discrete data (9)–(10) and take $q \geqslant m$, we derive estimates of the local truncation error of order $\Delta t|\Delta x|^{2m+2}$ for even derivatives and $\Delta t|\Delta x|^{2m+1}$ for odd derivatives. However, translating stability from the HB semi-norm to L^2 is not straightforward, and, as discussed in [20], one can at best expect the convergence at order $2m$. Moreover, the energy and L^2 error bounds derived in [20] degrade in time by factors of t^2 and t^3, respectively; we have never observed this growth in numerical experiments. However, it is observed in [20] that for m, even the conservative approximation to the acoustic system leads to convergence at order $2m + 2$ and an argument is presented in one-space dimension to explain it. The focus here is on methods with $m \geqslant 3$ and our experiments do not unambiguously determine if this phenomenon occurs though least squares fit to the convergence rate for $m = 4$ do generally exceed 10. One experiment with $m = 2$ does very clearly exhibit the convergence at order 6, and so we conjecture that the convergence rate is in fact $2m + 2$ for m even.

4 Numerical Experiments

Here we present some illustrations of the performance of the proposed methods for the transverse magnetic reduction of Maxwell's equations in two-space dimensions. In all our examples, we simply impose the periodicity in space. We note that for these simple domains, it is also straightforward to implement perfect electric conductor boundary conditions by imposing appropriate even and odd extensions of the electric fields at the boundary. This would be a primitive version of the compatibility boundary condition method mentioned above.

4.1 Dielectric Medium

We evolve solutions of the form

$$\begin{aligned} E_x &= -\frac{k}{\epsilon\omega}\sin(kx)\cos(ky)\cos(\omega t),\\ E_y &= \frac{k}{\epsilon\omega}\cos(kx)\sin(ky)\cos(\omega t),\\ H_z &= \sin(kx)\sin(ky)\sin(\omega t) \end{aligned}$$

with $(x, y) \in (-\pi, \pi)^2$, $\epsilon = \frac{5}{4}$, $\mu = \frac{4}{5}$, and $\omega = \sqrt{2}k$. We present two sets of experiments. The first is simply to examine the convergence rates for various values of m. The second is to compare the efficiency in terms of the total degrees-of-freedom required as well as the CPU time for problems of varying difficulty and error tolerances.

Convergence

We fix $k = 40$ and solve to $T = 100$. Since the wave speed is 1 and the wavelength is $2\pi/40$, a wave can travel approximately 636.6 wavelengths during the simulation and in time, there are 900.3 periods. Here we vary m from 3 to 6 and sample with mesh sizes in convenient increments starting with meshes which produce errors roughly from 1% to 10%. Precisely for $m = 3$, we take $\Delta x = \Delta y = 2\pi/N_G$ with $N_G = 125{:}25{:}275$. For $m = 4$, we take $N_G = 100{:}25{:}250$, for $m = 5$, $N_G = 50{:}25{:}200$, and for $m = 6$, $N_G = 40{:}20{:}160$. In our comparisons, we will always consider the degrees-of-freedom per wavelength for each coordinate direction. As the number of the degrees-of-freedom is $m + 1$, the ranges here begin with 12.5 for $m = 3, 4$, and 7.5 for $m = 5$, and 7.0 for $m = 6$. In all cases, we choose

$$\mathrm{CFL} = \frac{\Delta t}{\Delta x} = 0.9,$$

and use a temporal order $q = m + 2$. Recall that our stability proofs assume a much larger temporal order, $q = 3m + 2$, but our experiments show that $q = m + 2$ is sufficient for $m = 3, \cdots, 6$ and that increasing q does not improve the accuracy. In some experiments below, we use even higher values of m where we found that q needed to be $m + 3$ for the stability with $\mathrm{CFL} = 0.9$.

We approximate the L^2 error every time step by evaluating the Hermite solution onto a $2m \times 2m$ mesh in each cell and summing the results. For each cell $(\hat{j}_1, \hat{j}_2)$, set $\tilde{x}_{\hat{j}_1,k_1} = x_{j_1} + \Delta x(k_1 - 1)/(2m - 1)$, $\tilde{y}_{\hat{j}_2,k_2} = y_{j_2} + \Delta y(k_2 - 1)/(2m - 1)$ and compute

$$H^{\Delta x}_{z,\hat{j}_1,\hat{j}_2,k_1,k_2}(t_j) = \mathcal{I}_m H^h_z(\tilde{x}_{\hat{j}_1,k_1}, \tilde{y}_{\hat{j}_2,k_2}, t_j).$$

Then we define the relative error by

$$E(m, \Delta x) = \frac{1}{\pi\sqrt{N_T}}\left[\sum_{j=1}^{N_T}\frac{\Delta x\ \Delta y}{(2m-1)^2}\sum_{\hat{j}_1,\hat{j}_2,k_1,k_2}\left(\delta H_{z,\hat{j}_1,\hat{j}_2,k_1,k_2}(t_j)\right)^2\right]^{1/2}, \tag{57}$$

where

$$\delta H_{z,\hat{j}_1,\hat{j}_2,k_1,k_2}(t_j) = H^{\Delta x}_{z,\hat{j}_1,\hat{j}_2,k_1,k_2}(t_j) - H_z(\tilde{x}_{\hat{j}_1,k_1}, \tilde{y}_{\hat{j}_2,k_2}, t_j).$$

Here N_T is the number of steps. We are using π as the relative scale since it is the maximum L^2-norm of H_z and thus normalizing the errors by $\sqrt{\sum_{j=1}^{N_T}\pi^2}$. The results, shown in Fig. 1,

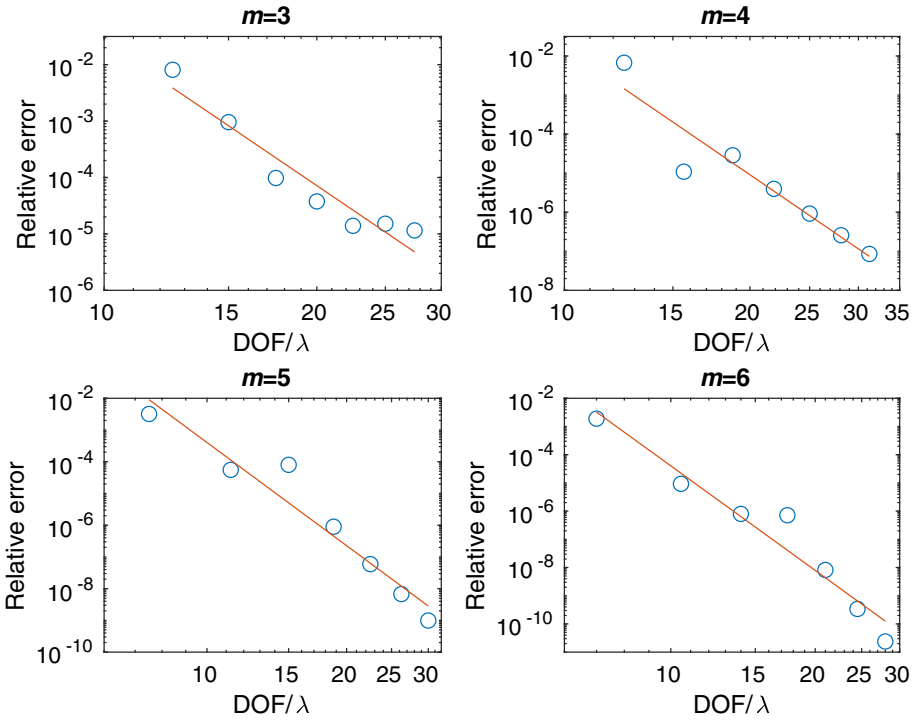

Fig. 1 Convergence for $m = 3, \cdots, 6$, $k = 40$, $T = 100$ in a dielectric medium. Errors are computed by comparing the Hermite interpolant of the numerical solution to the exact solution for each time step

Table 1 Observed convergence for $m = 3, \cdots, 6$ with $k = 40$ and $T = 100$ for the dielectric medium

m	DOF/λ	Fit rate
3	12.5–27.5	8.5
4	12.5–31.2	10.8
5	7.5–30	10.8
6	7–28	12.3

Here DOF/λ denotes the number of the degrees-of-freedom per wavelength in each coordinate direction, $N_G(m+1)/k$ where the mesh is $N_G \times N_G$. That is $\Delta x = \Delta y = 2\pi/N_G$. The error is computed by (57)

are sometimes choppy from mesh to mesh. We display a linear least squares fit to the log of the error as a function of the log of DOF/λ. This produces convergence rate estimates shown in Table 1. In all cases, these meet or exceed the theoretical rate of $2m$. For the cases $m = 3$ and $m = 4$, they are in fact consistent with $2m + 2$, but we do not claim that these methods have a theoretical convergence rate greater than $2m$.

The convergence arising from the various choices for m is directly compared in Fig. 2. The results in general show that for any particular error level, the larger values of m are more efficient in terms of the degrees-of-freedom required. We will further examine the efficiency question in detail for more challenging problems below.

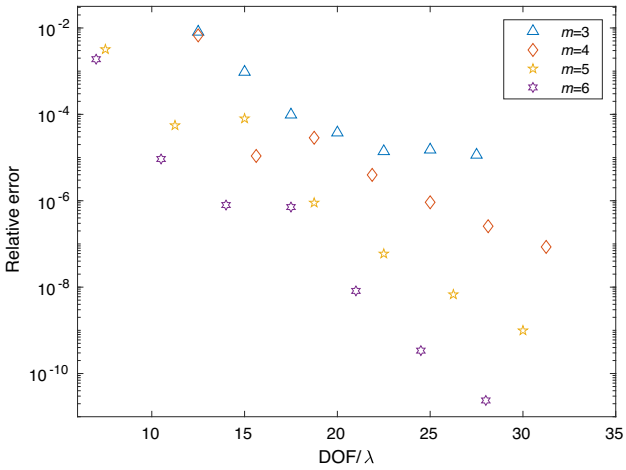

Fig. 2 Comparison of accuracy for $m = 3, \cdots, 6$, $k = 40$, $T = 100$ in the dielectric medium. Errors are computed by comparing the Hermite interpolant of the numerical solution to the exact solution for each time step

Efficiency

Here we consider larger values of k, $k = 50, 100, 200$, still evolving to $T = 100$. Varying $\Delta x = \Delta y = \frac{2\pi}{N_G}$ by sampling N_G in increments of 5 we determine the coarsest mesh for which the maximum recorded error relative to the maximum of the L^2-norm of H_z (π) is below the tolerances $\tau = 1\%$ and $\tau = 0.1\%$. Note that for these more challenging experiments, waves propagate for approximately 796, 1 592, and 3 183 wavelengths, respectively, corresponding to approximately 1 125, 2 251, and 4 502 temporal periods. As the problem difficulty increased, we also increased the values of m tested to $m = 7$ and $m = 8$ as the lower-order schemes became clearly less competitive. For these cases, we needed to set $q = m + 3$ to maintain the stability at CFL $= 0.9$. For comparison, we also tabulate the CPU times in seconds, which are obviously dependent on the implementation and hardware,[1] and varies somewhat with repeated runs. Nonetheless, we think the comparisons are still of interest. We remark that for the larger values of m, the cell widths themselves were larger than the wavelength.

The results, shown in Table 2, clearly illustrate the effectiveness of the high-order methods and the small computational overhead for Hermite methods as m is increased. In all cases, we achieve the desired tolerances with around 8–9 degrees-of-freedom per wavelength if we choose m large enough. Moreover, due to the fact that we can choose the CFL number independent of m, the large m runs were often faster. Although we are cognizant of the pitfalls in the interpretation of the timing data, we still believe that it is worth noting that in all but one case $m = 6$ achieved the tolerances in the least measured CPU time, and the increase in the number of the degrees-of-freedom per wavelength is quite mild; for example, for the 0.1% tolerance, $m = 6$ runs required 9.1, 9.1, and 9.3 as k was increased from 50 to 200.

[1] We implemented the method in Fortran 90, compiling with *gfortran* and an optimization -O4. The hardware is a single Intel i9-13900H core with 64 GiB memory.

Table 2 Values of N_G required for various values of m to achieve tolerances of 1% and 0.1% at $T = 100$ for various values of k

m	k	τ	N_G	DOF/λ	Time	$E_{\max}$
3	50	1E(−2)	200	16.0	7.2(2)	8.1(−3)
4	50	1E(−2)	140	14.0	5.5(2)	8.5(−3)
5	50	1E(−2)	70	8.4	1.3(2)	6.0(−3)
6	50	1E(−2)	55	7.7	8.8(1)	2.5(−3)
3	50	1E(−3)	250	20.0	2.9(3)	7.3(−4)
4	50	1E(−3)	185	18.5	1.1(3)	6.8(−4)
5	50	1E(−3)	85	10.2	2.1(2)	3.0(−4)
6	50	1E(−3)	65	9.1	1.5(2)	3.8(−4)
5	100	1E(−2)	160	9.6	1.4(3)	1.5(−2)
6	100	1E(−2)	120	8.4	9.3(2)	9.7(−3)
7	100	1E(−2)	100	8.0	9.5(2)	3.9(−3)
5	100	1E(−3)	170	10.2	1.7(3)	6.6(−4)
6	100	1E(−3)	130	9.1	1.2(3)	7.9(−4)
7	100	1E(−3)	115	9.2	1.2(3)	3.8(−4)
6	200	1E(−2)	250	8.8	9.0(3)	6.2(−3)
7	200	1E(−2)	200	7.9	8.4(3)	7.9(−3)
8	200	1E(−2)	180	8.1	1.7(4)	5.5(−3)
6	200	1E(−3)	265	9.3	9.5(3)	2.8(−4)
7	200	1E(−3)	230	9.2	1.2(4)	7.5(−4)
8	200	1E(−3)	195	8.8	1.8(4)	5.3(−4)

Here $E_{\max}$ is the maximum relative error over all time steps j as computed by the formula used in (57)

4.2 Dispersive Medium

As an example, we consider a single-term Lorentz model for the permittivity and approximate solutions of the form considered in [5]. Specifically, we take

$$\epsilon = \mu = 1, \quad \Omega_{e,1} = 1, \quad \omega_{e,1} = \sqrt{1.052\,\pi} \approx 1.818, \quad \gamma_{e,1} = 0.010\,7,$$

which can be obtained by scaling the model for the cubic silicon carbide listed in [15]. We will also carry out experiments for the Sellmeier model obtained by setting $\gamma_{e,1} = 0$.

Assuming 2π-periodicity, we again take $k = 40$ and $T = 100$ and approximate solutions of the form:

$$\begin{aligned}
E_x &= -\frac{1}{2k}\sin(kx)\cos(ky)\left(\omega\cos(\omega t) - \theta\sin(\omega t)\right)\mathrm{e}^{-\theta t},\\
E_y &= \frac{1}{2k}\cos(kx)\sin(ky)\left(\omega\cos(\omega t) - \theta\sin(\omega t)\right)\mathrm{e}^{-\theta t},\\
H_z &= \sin(kx)\sin(ky)\sin(\omega t)\mathrm{e}^{-\theta t},\\
K_x &= \frac{1}{2k\omega_{e,1}^2}\sin(kx)\cos(ky)\left(-2\omega\theta\cos(\omega t) + \left(2k^2+\theta^2-\omega^2\right)\sin(\omega t)\right)\mathrm{e}^{-\theta t},\\
K_y &= -\frac{1}{2k\omega_{e,1}^2}\cos(kx)\sin(ky)\left(-2\omega\theta\cos(\omega t) + \left(2k^2+\theta^2-\omega^2\right)\sin(\omega t)\right)\mathrm{e}^{-\theta t},
\end{aligned}$$

$$L_x = \frac{1}{2k\omega_{e,1}^2\left(\theta^2+\omega^2\right)}\sin(kx)\cos(ky)$$
$$\times\left(\left(\theta^2+\omega^2-2k^2\right)\omega\cos(\omega t)-\left(2k^2+\theta^2+\omega^2\right)\theta\sin(\omega t)\right)\mathrm{e}^{-\theta t},$$
$$L_y = -\frac{1}{2k\omega_{e,1}^2\left(\theta^2+\omega^2\right)}\cos(kx)\sin(ky)$$
$$\times\left(\left(\theta^2+\omega^2-2k^2\right)\omega\cos(\omega t)-\left(2k^2+\theta^2+\omega^2\right)\theta\sin(\omega t)\right)\mathrm{e}^{-\theta t},$$

where $z=-\theta+\mathrm{i}\omega$ is a root of the quartic equation

$$z^4+\gamma_{e,1}z^3+\left(2k^2+\omega_{e,1}^2+\Omega_{e,1}^2\right)z^2+2k^2\gamma_{e,1}z+2k^2\Omega_{e,1}^2=0.$$

For our choice of parameters, we compute the roots (labeled r for resonant and h for high frequency):

$$\theta_r = 0.005\,344\,476\,784\,229,\quad \omega_r = 0.999\,469\,550\,181\,686, \tag{58}$$
$$\theta_h = 0.000\,005\,523\,215\,771,\quad \omega_h = 56.597\,756\,028\,029\,032. \tag{59}$$

Setting $\gamma_{e,1}=0$, we have $\theta=0$ and

$$\omega_r^S = 0.999\,483\,839\,356\,918,\quad \omega_h^S = 56.597\,756\,029\,072\,784. \tag{60}$$

For the Lorentz model $\Gamma_V=0$, we need only evolve $\tilde{D}_W$ satisfying

$$\frac{\partial\tilde{D}_W}{\partial t} = -\gamma_{e,1}\begin{pmatrix}K_x\\K_y\end{pmatrix}. \tag{61}$$

The implicit Nordsieck method we use to evolve (61) employs polynomials of degree 6 which limits the formal method order to 6 in time. Nonetheless, we will use values of m ranging from 2 to 6 to understand how the discretization of the dissipative term affects the accuracy.

Obviously, the high-frequency solutions, H_z, of the Sellmeier model and the Lorentz model will be approximately equal up to $T=100$; their maximum relative difference is approximately 5×10^{-4}. However, we will see that our method performs differently in these two cases.

4.3 Resonant Case

As in the dielectric case, we test for convergence with m varying from 3 to 6. We fixed CFL $=0.9$, which led to stable results for the meshes tested. The meshes were chosen to have errors around 1% for the coarsest mesh and the mesh sizes changed by a convenient factor. Precisely for $m=3$, we use $N_G=100{:}25{:}250$, for $m=4$, $N_G=50{:}25{:}200$, for $m=5$, $N_G=50{:}25{:}200$, and for $m=6$, $N_G=30{:}20{:}150$.

The results, shown in Fig. 3, are again choppy from mesh to mesh. We display a linear least squares fit to the log of the error as a function of the log of DOF/λ. This produces convergence rate estimates shown in Table 3. Perhaps surprisingly, in almost all cases, these meet or exceed the theoretical rate of $2m$ for a dielectric medium or Sellmeier model, exceeding the theoretical rate of 6 of the approximation to the dissipative term in the Lorentz model. We suspect this is due to the contrast between the spatial and temporal frequencies; even with CFL $=0.9$, we are somewhat over resolved in time.

The convergence arising from the various choices for m is directly compared in Fig. 4. Again the results show that for any particular error level, the larger values of m are generally more efficient in terms of the degrees-of-freedom required.

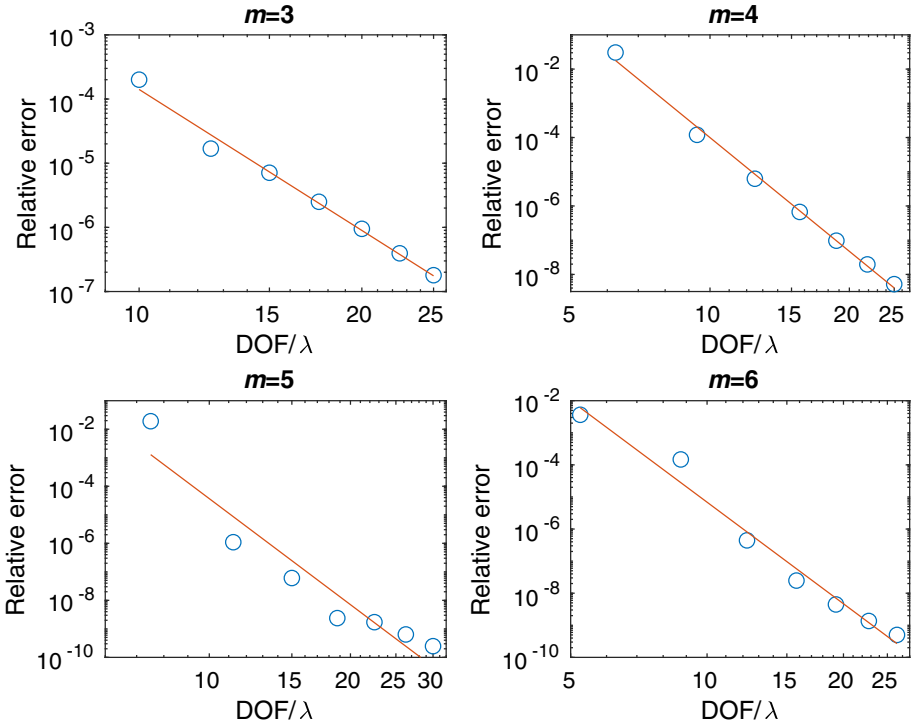

Fig. 3 Convergence for $m = 3, \cdots, 6$, $k = 40$, $T = 100$ for the near-resonant mode in a Lorentz medium. Errors are computed by comparing the Hermite interpolant of the numerical solution to the exact solution for each time step

Table 3 Observed convergence for $m = 3, \cdots, 6$ with $k = 40$ and $T = 100$ in the Lorentz model for the near-resonant mode

m	DOF/λ	Fit rate
3	10–25	7.3
4	6.25–25	11.0
5	7.5–30	12.4
6	5.25–26.25	10.5

Here DOF/λ denotes the number of degrees-of-freedom per wavelength in each coordinate direction, $N_G(m+1)/k$ where the mesh is $N_G \times N_G$. That is $\Delta x = \Delta y = 2\pi/N_G$. The error is computed by (57)

4.4 High-Frequency Case

We now consider the high-frequency solution of the Lorentz model with $k = 40$. Recall that the dissipation is nearly negligible in this case; the solution of the Sellmeier model obtained by setting $\gamma_{e,1} = 0$ agrees with the solution of the Lorentz model to more than three digits of accuracy, and so adding the dissipative term only improves the accuracy if we solve with a tolerance below 10^{-4}. Nonetheless, we find that the proposed method is limited by the sixth-order time-stepping scheme used in the treatment of the dissipative terms, and that nothing is gained by increasing m beyond 3. In addition, comparing the results with $m = 3$

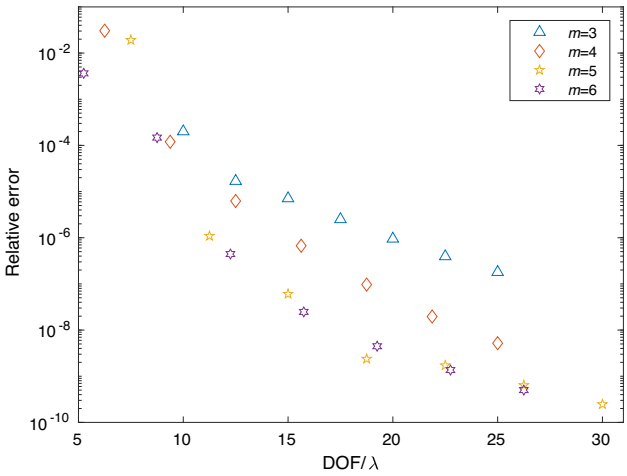

Fig. 4 Comparison of accuracy for $m = 3, \cdots, 6$, $k = 40$, $T = 100$ in the Lorentz medium for the near-resonant mode. Errors are computed by comparing the Hermite interpolant of the numerical solution to the exact solution for each time step

for the Lorentz model to those shown below for the Sellmeier model we see that the mesh must be refined by more than 50% to achieve comparable accuracies.

In Fig. 5, we examine the convergence for $m = 2$ and $m = 3$. For $m = 2$, we vary N_G from 200 to 800 and clearly observe the sixth-order convergence; the least squares fit produces an estimated rate of 6.2. For $m = 3$, we vary N_G from 150 to 450 but only observe the convergence for $N_G \geqslant 300$. The least squares fit to the last three data points yields an estimated convergence rate of 7.5.

The convergence arising for $m = 2, 3, 4$ is directly compared in Fig. 6. We observe that of the three choices $m = 4$ is the least efficient in terms of the degrees-of-freedom required for a given tolerance though there is some advantage to choosing $m = 3$.

4.5 Sellmeier Model

Lastly, we solve the Sellmeier model for the high-frequency mode. Here again we compare results for $m = 3, \cdots, 6$. The mesh sequences tested were $N_G = 150{:}25{:}300$ for $m = 3$, $100{:}25{:}250$ for $m = 4$, $50{:}25{:}200$ for $m = 5$, and $40{:}20{:}160$ for $m = 6$.

The results, shown in Fig. 7, are very similar to the dielectric and resonant cases. The least squares fit convergence rates produce convergence rate estimates shown in Table 4. In all cases, these are at least $2m$.

The convergence arising from the various choices for m is directly compared in Fig. 8. Again the results show that for any particular error level, the larger values of m are generally more efficient in terms of the degrees-of-freedom required.

5 Conclusions and Open Issues

In conclusion, we have proposed arbitrary-order energy-conserving Hermite discretizations of Maxwell's equations for both dielectric and dissipation-free dispersive media. For these

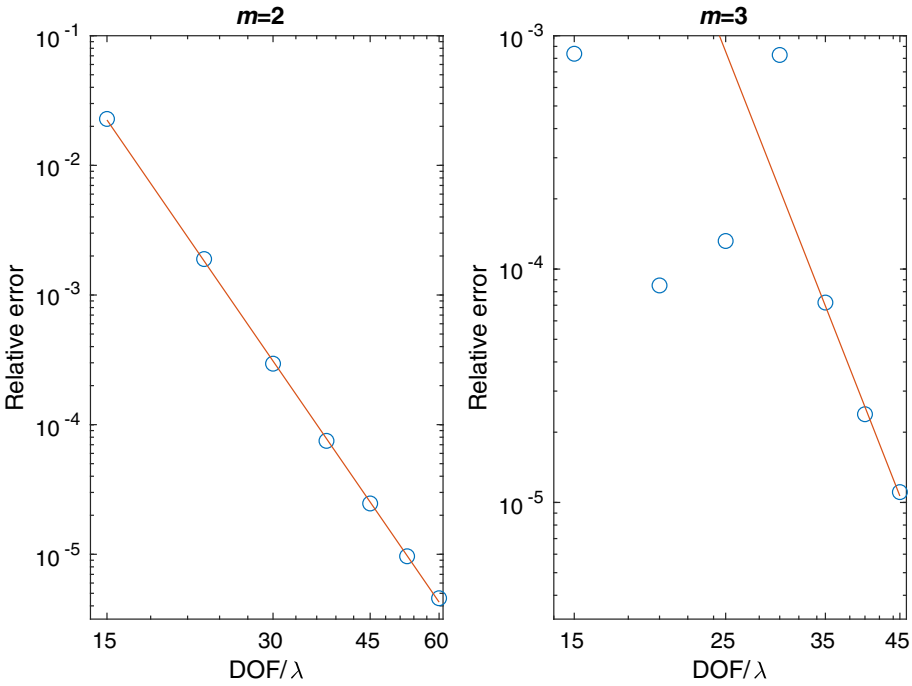

Fig. 5 Convergence for $m = 2, 3$, $k = 40$, $T = 100$ for the high-frequency mode in a Lorentz medium. Errors are computed by comparing the Hermite interpolant of the numerical solution to the exact solution for each time step

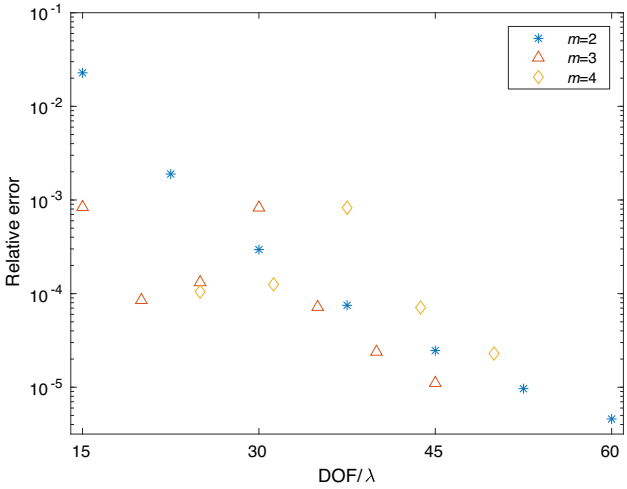

Fig. 6 Comparison of accuracy for $m = 2, 3, 4$, $k = 40$, $T = 100$ in the Lorentz medium for the high-frequency mode. Errors are computed by comparing the Hermite interpolant of the numerical solution to the exact solution for each time step

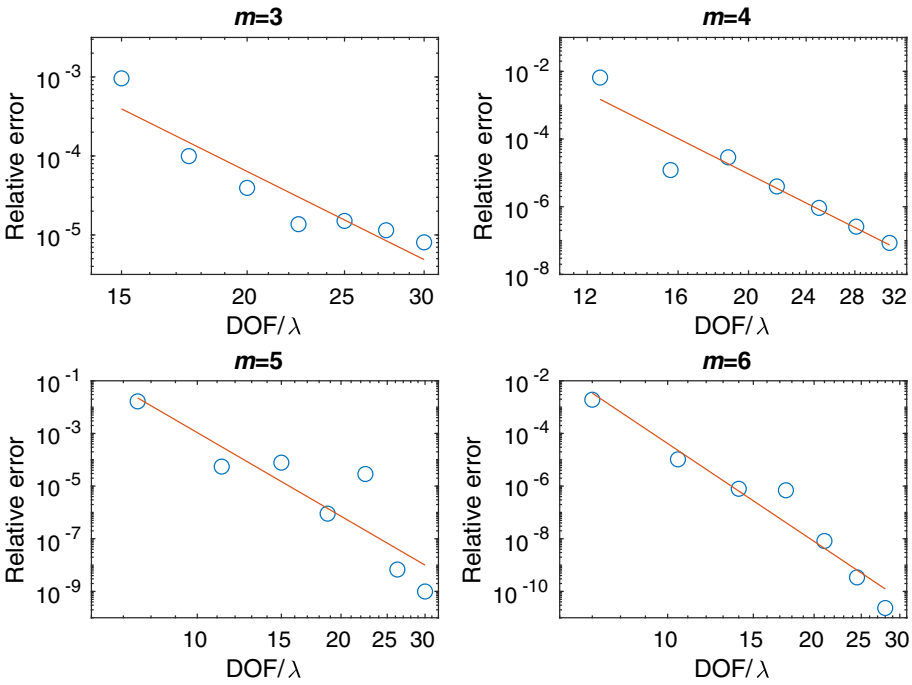

Fig. 7 Convergence for $m = 3, \cdots, 6$, $k = 40$, $T = 100$ for the Sellmeier model. Errors are computed by comparing the Hermite interpolant of the numerical solution to the exact solution for each time step

Table 4 Observed convergence for $m = 3, \cdots, 6$ with $k = 40$ and $T = 100$ for the Sellmeier model

m	DOF/λ	Fit rate
3	15–30	6.3
4	12.5–31.25	10.8
5	7.5–30	10.6
6	7–28	12.4

Here DOF/λ denotes the number of the degrees-of-freedom per wavelength in each coordinate direction, $N_G(m+1)/k$ where the mesh is $N_G \times N_G$. That is $\Delta x = \Delta y = 2\pi/N_G$. The error is computed by (57)

cases and with time-stepping of a sufficiently high order, we prove the stability for $c\frac{\Delta t}{\Delta x} < 1$ independent of order. Numerical experiments show that the high-order schemes are capable of accurately propagating waves over thousands of wavelengths with 9 or fewer degrees-of-freedom per wavelength. We also show how to include the dissipation in the dispersive models though this limits the formal order of the accuracy and, in some cases, significantly degrades efficiency.

From a practical perspective, the future work will focus on implementations in more complex geometry incorporating boundary and interface conditions and on exploiting the locality of the evolution formulas for the efficient implementation on current computer architectures. We will also consider if the possibility of using the high-order dissipative Hermite methods [7] is worthwhile for Lorentz models.

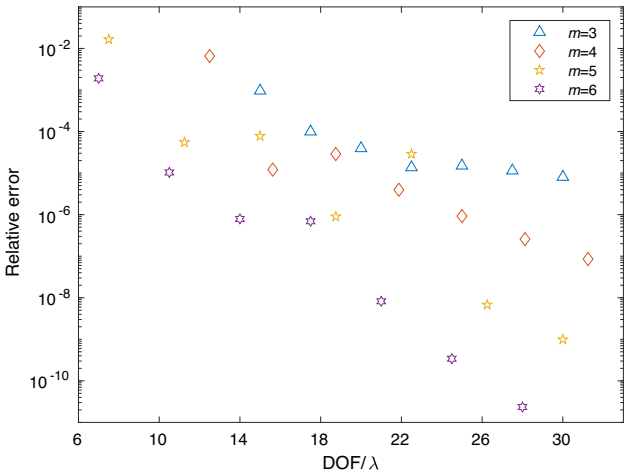

Fig. 8 Comparison of accuracy for $m = 3, \cdots, 6$, $k = 40$, $T = 100$ for the Sellmeier model. Errors are computed by comparing the Hermite interpolant of the numerical solution to the exact solution for each time step

In terms of the theory, the fundamental open issues are a complete analysis of the convergence in L^2 and of the stability of the boundary and interface approximations.

Acknowledgements This work was funded in part by the National Science Foundation Grants DMS-2012296, DMS-2309687, and DMS-2210286. Any opinions, findings, and conclusions or recommendations expressed in this material are those of the authors and do not necessarily reflect the views of the NSF. We also thank the anonymous referee whose suggestions improved our presentation of the results.

Code Availability The source codes used to produce the results in this paper are available by request to the corresponding author.

Declarations

Conflict of Interest The authors declare there is no conflict of interest.

References

1. Appelö, D., Chen, R., Hagstrom, T.: A hybrid Hermite-discontinuous Galerkin method for hyperbolic systems with applications to Maxwell's equations. J. Comput. Phys. **257**, 501–520 (2013)
2. Appelö, D., Hagstrom, T.: Solving PDEs with Hermite interpolation. In: Lecture Notes in Computational Science, pp. 31–49. Springer, Berlin (2015)
3. Appelö, D., Hagstrom, T., Vargas, A.: Hermite methods for the scalar wave equation. SIAM J. Sci. Comput. **40**, 3902–3927 (2018)
4. Banks, J.W., Buckner, B., Henshaw, W., Jenkinson, M., Kildeshev, A., Kovacic, G., Prokopeva, L., Schwendeman, D.: A high-order accurate scheme for Maxwell's equations with a Generalized Dispersive Material (GDM) model and material interfaces. J. Comput. Phys. **412**, 109424 (2020)
5. Bokil, V., Gibson, N.: Convergence analysis of Yee schemes for Maxwell's equations in Debye and Lorentz dispersive media. Int. J. Numer. Anal. Mod. **11**, 657–687 (2014)
6. Byrne, G.D., Hindmarsh, A.C.: A polyalgorithm for the numerical solution of ordinary differential equations. ACM Trans. Math. Softw. **1**, 71–96 (1975)
7. Goodrich, J., Hagstrom, T., Lorenz, J.: Hermite methods for hyperbolic initial-boundary value problems. Math. Comput. **75**, 595–630 (2006)
8. Hairer, E., Norsett, S., Wanner, G.: Solving Ordinary Differential Equations I. Nonstiff Problems. Springer, New York (1992)
9. Holland, R.: Finite-difference solution of Maxwell's equations in generalized nonorthogonal coordinates. IEEE Trans. Nucl. Sci. **30**, 4589–4591 (1983)
10. Jiang, Y., Sakkaplangkul, P., Bokil, V., Cheng, Y., Li, F.: Dispersion analysis of finite difference and discontinuous Galerkin schemes for Maxwell's equations in linear Lorentz media. J. Comput. Phys. **394**, 100–135 (2019)
11. Joly, P.: Variational methods for time-dependent wave propagation problems. In: Ainsworth, M., Davies, P., Duncan, D., Martin, P., Rynne, B. (eds.) Topics in Computational Wave Propagation, pp. 201–264. Springer, Berlin (2003)
12. Law, Y.-M., Appelö, D.: The Hermite-Taylor correction function method for Maxwell's equations. Commun. Appl. Math. Comput. **7**, 347–371 (2023). https://doi.org/10.1007/s42967-023-00287-5
13. Loya, A.A., Appelö, D., Henshaw, W.D.: High order accurate Hermite schemes on curvilinear grids with compatibility boundary conditions. J. Comput. Phys. **522**, 113597 (2025)
14. Mai, W., Campbell, S.D., Whiting, E.B., Kang, L., Werner, P.L., Chen, Y., Werner, D.H.: Prismatic discontinuous Galerkin time domain method with an integrated generalized dispersion model for efficient optical metasurface analysis. Opt. Mater. Express **10**, 2542–2559 (2020)
15. Palik, E.D.: Handbook of Optical Constants of Solids II. Academic Press, San Diego (1998)
16. Prokopeva, L., Borneman, J., Kildishev, A.: Optical dispersion models for time-domain modeling of metal-dielectric nanostructures. IEEE Trans. Magn. **47**, 1150–1153 (2011)
17. Qiang, R., Bao, H., Campbell, S.D., Prokopeva, L.J., Kildishev, A.V., Werner, D.H.: Continuous-discontinuous Galerkin time domain (CDGTD) method with generalized dispersive material (GDM) model for computational photonics. Opt. Express **26**, 29005–29016 (2018)
18. Shi, C., Li, J., Shu, C-W.: Discontinuous Galerkin methods for Maxwell's equations in Drude metamaterials on unstructured meshes. J. Comput. Appl. Math. **342**, 147–163 (2018)
19. Vargas, A., Chan, J., Hagstrom, T., Warburton, T.: GPU acceleration of Hermite methods for simulation of wave propagation. In: Lecture Notes in Computational Science, pp. 357–368. Springer, Berlin (2017)
20. Vargas, A., Hagstrom, T., Chan, J., Warburton, T.: Leapfrog time-stepping for Hermite methods. J. Sci. Comput. **30**, 289–314 (2019)
21. Yang, W., Huang, Y., Li, J.: Developing a time-domain finite element method for the Lorentz metamaterial model and applications. J. Sci. Comput. **68**, 438–463 (2016)